



**Predicted IL-18/IL-18R Binding Improvement Through Protein  
Interface Modification with Computer-aided Design**

**Napat Prompat**

**A Thesis Submitted in Partial Fulfillment of the Requirements for the  
Degree of Master of Science in Biomedical Sciences**

**Prince of Songkla University**

**2021**

**Copyright of Prince of Songkla University**



**Predicted IL-18/IL-18R Binding Improvement Through Protein  
Interface Modification with Computer-aided Design**

**Napat Prompat**

**A Thesis Submitted in Partial Fulfillment of the Requirements for the  
Degree of Master of Science in Biomedical Sciences**

**Prince of Songkla University**

**2021**

**Copyright of Prince of Songkla University**

**Thesis Title** Predicted IL-18/IL-18R binding improvement through protein interface modification with computer-aided design

**Author** Napat Prompat

**Major Program** Biomedical Sciences

---

**Major Advisor**

.....  
 (Asst. Prof. Dr. Varomyalin Tipmanee)

**Examining Committee:**

.....Chairperson  
 (Asst. Prof. Dr. Thanyada Rungrotmongkol)

.....Committee  
 (Prof. Dr. Surasak Sangkhathat M.D.)

.....Committee  
 (Asst. Prof. Dr. Varomyalin Tipmanee)

.....Committee  
 (Dr. Niran Roongsawang)

The Graduate School, Prince of Songkla University, has approved this thesis as partial fulfillment of the requirements for the Master of Science Degree in Biomedical Sciences

.....  
 (Prof. Dr. Damrongsak Faroongsarng)

Dean of Graduate School

This is to certify that the work here submitted is the result of the candidate's own investigations. Due acknowledgement has been made of any assistance received.

.....Signature

(Asst. Prof. Dr. Varomyalin Tipmanee)  
Major Advisor

.....Signature

(Mr. Napat Prompat)  
Candidate

I hereby certify that this work has not been accepted in substance for any degree, and is not being currently submitted in candidature for any degree.

.....Signature

(Mr. Napat Prompat)

Candidate

**ชื่อวิทยานิพนธ์** การปรับปรุงประสิทธิภาพการจับของโปรตีนอินเตอร์ลิวคิน-18 กับ โปรตีนตัวรับ  
ผ่านการดัดแปลงบริเวณอินเตอร์เฟสด้วยวิธีการใช้คอมพิวเตอร์ช่วยออกแบบ

**ผู้เขียน** นายณภัทร พรหมพัฒน์

**สาขาวิชา** ชีวเวชศาสตร์

**ปีการศึกษา** 2563

### บทคัดย่อ

การรักษาโรคมะเร็งด้วยวิธีภูมิคุ้มกันบำบัดโดยการใช้ไซโตไคน์ หรือ Cytokine-mediated immunotherapy เป็นแนวทางหนึ่งในการรักษาโรคมะเร็งที่มีประสิทธิภาพผ่านการกระตุ้นระบบภูมิคุ้มกันของร่างกายให้ตอบสนองต่อการยับยั้งและกำจัดเซลล์มะเร็ง อินเตอร์ลิวคิน-18 เป็นไซโตไคน์ได้รับการรายงานถึงความสำคัญในการกระตุ้นภูมิคุ้มกันต้านมะเร็งโดยทำหน้าที่ส่งเสริมการทำงานของเซลล์เม็ดเลือดขาวชนิด Natural killer cells และ Cytotoxic T lymphocytes ในการยับยั้งเซลล์มะเร็งให้มีประสิทธิภาพมากยิ่งขึ้น การทำงานของอินเตอร์ลิวคิน-18 จำเป็นต้องอาศัยการจับในบริเวณที่มีความจำเพาะกับโมเลกุลตัวรับบนเซลล์เป้าหมายและการดัดแปลงกรดอะมิโนที่บริเวณดังกล่าวจัดเป็นแนวทางที่น่าสนใจในการพัฒนาประสิทธิภาพของอินเตอร์ลิวคิน-18 งานวิจัยนี้มีจุดประสงค์เพื่อออกแบบและทำนายการเปลี่ยนแปลงกรดอะมิโนที่มีแนวโน้มที่จะเพิ่มประสิทธิภาพการทำงานของอินเตอร์ลิวคิน-18 ด้วยเทคนิคทางคอมพิวเตอร์ในการคำนวณค่าพลังงานอิสระในการจับร่วมกับการจำลองแบบทางพลวัตเชิงโมเลกุลโดยใช้โครงสร้างสามมิติของอินเตอร์ลิวคิน-18 ที่จับอยู่กับตัวรับเป็นแม่แบบในการออกแบบ ผู้วิจัยได้ทำการเปลี่ยนกรดอะมิโนของอินเตอร์ลิวคิน-18 ตรงบริเวณเข้าจับกับตัวรับเป็นกรดอะมิโนรูปแบบต่างๆและคำนวณค่าพลังงานอิสระในการจับด้วยโปรแกรม FoldX โดยการกลายพันธุ์ที่สนใจจะเลือกจากหลักเกณฑ์ คือ 1) ค่าพลังงานที่ต่ำที่สุด และ

2) การสังเกตเชิงโครงสร้าง จากการศึกษาพบว่ามีการกลายพันธุ์ที่มีศักยภาพควรให้ค่าพลังงานที่เหมาะสมและยังคงรักษาเสถียรภาพของโครงสร้างจำนวน 4 รูปแบบจากทั้งหมด 227 รูปแบบ ได้แก่ E6M, E6M+N111S+R131G, E6M+K129M+R131G และ E6M+N111S+K129M+R131G โดยการเข้าจับกันของโปรตีนทั้งสองผ่านทางแรงยึดเหนี่ยวที่สำคัญคือแรงประจุไฟฟ้าสถิตส่งผลให้เกิดการเพิ่มขึ้นของความสามารถการจับกันและเสถียรภาพของโปรตีนเมื่อเทียบกับโปรตีนอินเตอร์ลิวคิน-18 ปกติ ทั้งนี้ผู้วิจัยได้ศึกษาผลของการเปลี่ยนกรดอะมิโนของทั้ง 4 รูปแบบต่อโครงสร้างและพฤติกรรมเชิงพลวัตของอินเตอร์ลิวคิน-18 ด้วยเทคนิคการจำลองแบบทางพลวัตเชิงโมเลกุลที่อุณหภูมิ 310 เคลวิน และความดัน 1 ความดันบรรยากาศ พบว่าการกลายพันธุ์ดังกล่าวไม่ส่งผลกระทบต่อโครงสร้างโดยรวมของอินเตอร์ลิวคิน-18 แต่เพิ่มความยืดหยุ่นในบริเวณโครงสร้างรูปห่วง ( $\beta 8$ - $\beta 9$  hairpin loop) นอกจากนี้การกลายพันธุ์ทั้ง 4 แบบยังส่งผลต่อประสิทธิภาพในการทำงานของอินเตอร์ลิวคิน-18 ได้ โดยสรุปแล้วงานวิจัยนี้ได้นำเสนอวิธีการทางคอมพิวเตอร์ซึ่งอาศัยความรู้เชิงโครงสร้างของโปรตีนที่เป็นประโยชน์ในการออกแบบและพัฒนาอินเตอร์ลิวคิน-18 ให้มีศักยภาพและประสิทธิภาพมากยิ่งขึ้น

**คำสำคัญ:** การรักษาโรคมะเร็งด้วยวิธีภูมิคุ้มกันบำบัดโดยการใช้ไซโตไคน์, อินเตอร์ลิวคิน-18, พลศาสตร์เชิงโมเลกุล, การออกแบบโดยอาศัยความรู้เชิงโครงสร้าง

**Thesis Title** Predicted IL-18/IL-18R binding improvement through protein interface modification with computer-aided design

**Author** Napat Prompat

**Major Program** Biomedical Sciences

**Academic Year** 2020

## ABSTRACT

Cytokine-mediated immunotherapy has rapidly emerged as an effective alternative approach for cancer treatment by modulating the anti-tumor response. Interleukin-18 (IL-18) has considered as a promising cancer therapeutic agent due to the ability of cytokine to inhibit cancer by enhancing natural killer (NK) cell and cytotoxic T cell responses. Since the activity of IL-18 required the specific binding to IL-18 receptors, the modification of binding residue at the interface of proteins is an attractive strategy for IL-18 activity enhancement. An aim of this study was thus to design and predict mutations increasing the activity of IL-18 through the integration of computational structure-based energy calculation and molecular dynamic simulations, using a crystal structure of human IL-18 in complex with the receptor as a template. We performed *in silico* saturation mutagenesis by mutating each of the unfavorable interface binding residues of IL-18. The relative free energy changes upon mutation ( $\Delta\Delta G$ ) were computed using FoldX algorithm. An interested mutation was selected based on two criteria: (1) the most favorable free energy contribution, and (2) the structural conservation. From total 227 possible mutations, four potential mutations were finally obtained. The selected four candidate mutations were E6M, E6M+N111S+R131G, E6M+K129M+R131G, and E6M+N111S+K129M+R131G could increase the receptor binding affinity and stability compared to the wild-type. The main interaction was due to the electrostatic interaction. These *in silico* acquired mutations were further investigated their impact on the overall structure and dynamic behavior using molecular dynamics simulation at 310 K and 1 atm. MD simulations demonstrated that the predicted mutation on IL-18 had no influence on the overall conformation stability, but increased flexibility in the  $\beta 8$ - $\beta 9$  hairpin loop. Furthermore, the dynamic behavior suggested that four mutation candidates could

alter the biological activity of IL-18. In summary, this study offered a computer-aided design strategy, which was a beneficial use of the design and development of IL-18 for increasing its cytokine potency and efficiency.

**KEYWORDS:** Cytokine-mediated immunotherapy, Interleukin-18, Molecular dynamics simulation, Structure-guided design

## ACKNOWLEDGEMENT

First and foremost, I would like express my very great appreciation to my supervisor, Asst. Prof. Dr. Varomyalin Tipmanee, who always supports and encourages during my master's degree program and also gave me the valuable guidance and opportunity throughout my study. His vision, sincerity and motivation have deeply inspired me. It was a great privilege and honor to work and study under his guidance. My appreciation is also expressed to Dr. Jirakrit Saetang for his kindness, guidance, support, and encouragement throughout this thesis. He gave me the opportunity to explore and improve and skill and knowledge that is so important for my career path in the future. Without their kindness and cheerfulness, this thesis could not be accomplished.

My gratitude is to Prof. Dr. Surasak Sangkhathat at Department of Surgery, Faculty of Medicine, Prince of Songkla Univeristy, Dr. Niran Roongsawang at National Center for Genetic Engineering and Biotechnology, National Science and Technology Development Agency for help in providing technical guidance and kind suggestions. I also would like to thank Asst. Prof. Dr. Thanyada Rungrotmongkol, my committee chair for the thoughtful comments and valuable suggestions to improve the quality of my thesis. In addition, my special thanks are extended to Ms. Chariya Peeyatu and Ms. Natnaree Sangkaew for their advices in molecular cloning and protein expression techniques.

I would like to thank all members and instructors in the Department of Biomedical Sciences, Faculty of Medicine, Prince of Songkla University who always motivated and provided me their assistance during my master's degree study.

Finally, I would like to express my deepest appreciation to my parents and other members of my family for their undying love, understanding, and everything giving throughout my life. Thank you everyone for giving me strength to reach for the stars and chase my dreams.

Napat Prompat

## CONTENTS

	<b>Page</b>
Abstract (Thai) .....	v
Abstract (English) .....	vii
Acknowledgement .....	ix
Contents .....	x
List of Tables .....	xii
List of Figures .....	xiii
List of Abbreviation and Symbols .....	xv
<b>Chapter</b>	
1. Introduction.....	1
Background of immunotherapy in cancer treatment .....	1
Role of IL-18 in cancer immunotherapy .....	3
Strategy to improve the biological activity of IL-18 by using site-directed mutagenesis .....	7
Computational approaches for designing therapeutic proteins and peptides .....	9
Template-based design .....	9
<i>De novo</i> protein design .....	11
Objectives.....	14
2. Research methodology .....	15
Schematic overview .....	15
Computational resources .....	15
<i>In-silico</i> mutagenesis and energy decomposition .....	17
Structure preparation .....	17
Energy decomposition .....	17
<i>In-silico</i> mutagenesis .....	17
Analysis of relative binding free energy change upon mutation .....	18
Statistical analysis.....	18
Molecular dynamics (MD) simulation .....	18
System preparation .....	18
Energy minimization .....	19

## CONTENTS (CONTINUED)

Canonical (NVT) ensemble .....	19
Isobaric-Isothermal (NPT) ensemble .....	20
Trajectory analysis .....	20
Root mean square deviation (RMSD) .....	20
Root mean square fluctuation (RMSF).....	21
Distance pattern .....	21
Hydrogen bonding analysis .....	21
3. Result and discussion .....	22
Preliminary design of IL-18 using interaction-based point mutation .....	22
<i>In silico</i> design of IL-18 .....	22
Conformational analysis of IL-18 MD trajectory .....	23
Binding affinity evaluation.....	25
Per-residue decomposition energy .....	26
Contribution analysis of amino acid at IL-18/IL-18R interface.....	27
Validation of the computational approach .....	30
<i>In silico</i> screening of favorable mutation.....	35
Single point mutation study.....	35
Double mutation study.....	40
Multiple mutation study .....	41
Selection of favorable mutation.....	43
MD simulation analysis of mutations .....	44
Conformational stability analysis .....	44
Structural comparison.....	45
Hydrogen bond analysis .....	47
Structural flexibility analysis.....	49
Binding interaction analysis .....	51
4. Conclusion .....	57
5. References .....	59
6. Appendices.....	66
7. Vitae.....	83

## LIST OF TABLES

Tables	Pages
1. Anti-tumor properties of IL-18 in preclinical models.....	5
2. Biological activity of the mutants compared with IL-18 wild type.....	8
3. Summary of recent computationally designed proteins and peptides and their therapeutic applications.....	13
4. Binding affinity and biological activity of wild-type and mutant IL-18 structures.....	26
5. Comparison of experimental activity and <i>in silico</i> predicted relative free energy ( $\Delta\Delta G$ ) in human IL-18.....	31
6. <i>In silico</i> predicted relative free energy ( $\Delta\Delta G$ ) of single point mutation study.....	39
7. <i>In silico</i> predicted relative free energy ( $\Delta\Delta G$ ) of double mutation study.....	40
8. <i>In silico</i> predicted relative free energy ( $\Delta\Delta G$ ) of multiple mutation study.....	42
9. Binding interactions between the E6M mutant/IL-18R interfaces at binding site I, II and III.....	51
10. Binding interactions between the E6M+K129M+R131G mutant/IL-18R interfaces at binding site I, II and III.....	52
11. Binding interactions between the E6M+N111S+R131G mutant/IL-18R interfaces at binding site I, II and III.....	53
12. Binding interactions between the E6M+N111S+K129M+R131G mutant/IL-18R interfaces at binding site I, II and III.....	54

## LIST OF FIGURES

Figures	Pages
1. Structure of IL-18 and IL-18R $\alpha$ binding.....	6
2. Overview of template-based structure modeling protein design.....	10
3. Workflow of <i>de novo</i> computational protein design.....	12
4. Study overview shows a strategy to acquire the effective mutation candidate of IL-18.....	16
5. Structural comparison between wild-type and N41D mutant.....	23
6. Root-mean-square deviation (RMSD) from MD simulation of all IL-18 structures in Angstrom units.....	24
7. Root-mean-square fluctuation (RMSF) from MD simulation of all IL-18 structures in Angstrom units.....	25
8. Decomposition binding free energy of each residue of IL-18.....	27
9. Schematic representations of the interaction profiles between IL-18/IL-18R $\alpha$ complex.....	28
10. Per residue energy decomposition of the key amino acid at binding site I and II of IL-18.....	29
11. Per residue free energy contribution of IL-18 in the IL-18/IL-18R interface.....	30
12. Correlation between relative activities of IL-18 and the predicted binding free energies of IL-18/IL-18R complex.....	33
13. Correlation between relative activities of IL-18 and the predicted free energies of folding of IL-18/IL-18R complex.....	33
14. Correlation between relative activities of IL-18 and the predicted free energies of folding of IL-18.....	34
15. Heat map of the predicted free energy of binding of IL-18 upon mutation.....	36
16. Heat map of the predicted free energy of folding of IL-18/IL-18R complex upon mutation.....	37

## LIST OF FIGURES (CONTINUED)

<b>Figures</b>	<b>Pages</b>
17. Heat map of the predicted free energy of folding of IL-18 upon mutation.....	38
18. 3D structure of IL-18 in complex with IL-18R $\alpha$ . ....	44
19. Root-Mean-Square Deviation (RMSD) plots from the 150 ns MD simulations of all IL-18 structures .....	45
20. Average distance pattern in Angstrom units of all atoms in each IL-18 structures during MD simulation.....	46
21. Superimposition of the IL-18 structures with IL-18R $\alpha$ during MD simulation.....	47
22. Hydrogen bond profiles of IL-18 structures during MD simulation .....	48
23. Root-Mean-Square fluctuation (RMSF) plots of IL-18 structures during MD simulation.....	49
24. Superimposition of the IL-18 structures with IL-18R $\beta$ during MD simulation.....	50
25. Binding interaction of IL-18 with E6M+N111S+K129M+R131G mutation and IL-18R $\alpha$ at the receptor binding site I and II.....	55
26. Binding interaction of IL-18 with E6M+N111S+K129M+R131G mutation and IL-18R $\beta$ at the receptor binding site III.....	56

## LIST OF ABBREVIATION AND SYMBOLS

### Acronym

APCs	Antigen-presenting cells
AMBER	Assisted Model Building with Energy Refinement
CTLA-4	Cytotoxic T lymphocytes-associated protein 4
IFN- $\gamma$	Interferon-gamma
IL-18	Interleukin-18
IL-18R	Interleukin-18 receptor
MD	Molecular dynamics
MHC	Major Histocompatibility complex
NMR	Nuclear magnetic resonance
NPT	Isothermal–isobaric ensemble
NVT	Canonical ensemble
PDB	Protein Data Bank
PD-1	Programmed cell death protein 1
RCSB	Research Collaboratory for Structural Bioinformatics
RMSD	Root-mean-square deviation
RMSF	Root-mean-square fluctuation
TAA	Tumor-associated antigens
VMD	Visual Molecular Dynamics
X-ray	X-ray crystallography
3D	Three dimensional

### Amino acids

Ala	A	Alanine
Arg	R	Arginine
Asn	N	Asparagine
Asp	D	Aspartic acid (Aspartate)

Cys	C	Cysteine
Gln	Q	Glutamine
Glu	E	Glutamic acid (Glutamate)
Gly	G	Glycine
His	H	Histidine
Ile	I	Isoleucine
Leu	L	Leucine
Lys	K	Lysine
Met	M	Methionine
Phe	F	Phenylalanine
Pro	P	Proline
Ser	S	Serine
Thr	T	Threonine
Typ	W	Tryptophan
Tyr	Y	Tyrosine
Val	V	Valine

### **Greek letters and units**

$\beta$	Beta
$\Delta$	Delta
$\gamma$	Gamma
$\mu$	Micro
fs	Femtosecond
ns	Nanosecond
ps	Picosecond
K	Kelvin
Kcal	kilocalorie
Å	angstrom or $10^{-10}$ meter

## CHAPTER 1

### INTRODUCTION

#### 1.1 Background of immunotherapy in cancer treatment

Immunotherapy, immune-based treatment has emerged as a promising approach for cancer therapy and shown its great potential for treating human cancers due to selectivity and long-lasting effects (Koury et al., 2018). The immunotherapy also shows great progress toward a cancer treatment, such as immune checkpoint blockade agents, monoclonal antibodies, cancer vaccines, oncolytic viruses, adoptive cell therapy, and cytokine-mediated immunotherapy (Murphy, 2015). Immunotherapy is a potent therapeutic approach that relies on the host immune system to target and eliminate foreign invaders including bacteria, viruses, and particularly malignant cells (Farkona et al., 2016). Many studies later attempted to use microorganisms as a strategy of cancer treatment (Hoption et al., 2003; Morales et al., 2016). These approaches could be however potentially life-threatening due to the complication of bacterial infection.

The immune system recognizes tumor-associated antigens from transplanted tumor and promotes the anti-tumor immune responses of its existence. The hypothesis termed “cancer immunosurveillance” was established according to these immune mechanisms. (Morales et al., 2016; Oiseth & Aziz, 2017). The basis of immunosurveillance can distinguish self-antigens from others by antigen recognition via CD4<sup>+</sup> T cells toward major histocompatibility complex (MHC) molecules presented on the cell surface. Similarly, tumor cells are expressed tumor-associated antigens (TAAs) on the tumor cell surface. DCs serve as antigen-presenting cells to activate anti-cancer immune responses, by presenting the tumor antigens to the immune effector cells via MHC class I and class II, followed by the stimulation of anti-cancer response. The anti-cancer response activates CD4<sup>+</sup> T cells and CD8<sup>+</sup> T cells to recognize and eliminate cancer cells.

Moreover, the activation of cellular immunity due to anti-tumor state requires co-stimulatory signals that play a major role in facilitating T cells proliferation and

differentiation through the interaction of co-stimulatory receptor CD28 of T cells and a ligand, B7-1 on APC surface (Oiseth & Aziz, 2017). In spite of the well-organized tumor immunosurveillance system, the neoplastic cells are able to escape immune destruction. One important principle which clarified the understanding of immune evasion in cancer is related to the process termed “cancer immunoediting” (Morales et al., 2016). Cancer immunoediting proposes that the immune system not only involves defense mechanisms against malignant transformation in nascent transformed cells but also contributes significantly to the progression of tumors. Three major phases of cancer immunoediting process consists of elimination phase (also known as cancer immunosurveillance), equilibrium phase, and escape phase, respectively (Mittal et al., 2014; Smyth et al., 2006).

Researchers have recently succeeded in unleashing the potential of immunotherapy by targeting immune checkpoint pathways in programmed cell death protein 1 (PD-1) and cytotoxic T lymphocyte-associated protein 4 (CTLA-4). These strategies have proven to be a new frontier in cancer therapeutic approach that has revitalized the field of immune-based treatment, the so-called “cancer immunotherapy”. Among the immunotherapeutic strategies, cytokine therapy are emerging as a potential approach for cancer treatment through the manipulation of innate and adaptive immunity against cancer cells (Farkona et al., 2016; Zhang & Chen, 2018).

Cytokines act as immune modulators to provide cell-to-cell communication and regulation of immunological activities of immune cells in innate and adaptive immune response, for example, IL-2, IL-7, IL-12, IL-15, IL-21, GM-CSF, and IFN- $\alpha$ . (Waldmann, 2018) Released cytokine from immune cells binds its specific receptor(s) on the target cell surface. The binding subsequently activates gene transcription in intracellular signaling pathways to promote proliferation and differentiation of immune effector cells, such as NK cells, CD4<sup>+</sup> T cells, CD8<sup>+</sup> T cells, and DCs. Although cytokines are identified as nonspecific immunotherapy, they play important roles in potentiating the host immune response, providing synergistic efficiency among immunotherapeutic strategies, and inhibiting the immunosuppressive activity in cancer patients (Smyth et al., 2004).

## 1.2 Role of IL-18 in cancer immunotherapy

One of interesting cytokine candidates for immunotherapy is an interleukin-18 (IL-18), an 18 kDa immunostimulatory cytokine. IL-18 was primarily secreted by macrophages and encoded by the IL18 gene on chromosome 11q3.1 (Dinarello, 1999). IL-18 plays important roles in anti-tumor immune responses including the activation and proliferation of T cells, the induction of IFN- $\gamma$  production in natural killer (NK) cells, and the regulation of several cytokines in both innate and adaptive immunity against cancer cells, leading to the enhancement of patient's immune responses and tumor regression (Lee & Margolin, 2011).

Generally, IL-18 is first produced as a biologically inactive 24 kDa molecule, termed pro-IL-18. These inactive precursors require proteolytic cleavage enzymes for processing into the mature IL-18 (mat-IL-18) by using the intracellular cysteine protease caspase-1 (caspase-1), also known as IL-1 converting enzyme (ICE). Finally, an inactive pro-IL-18 is processed by caspase-1 into the active form (mat-IL-18) and subsequently secreted to the cellular environment (Dinarello, 1999; Nakanishi, 2018). IL-18 acts as a potent interferon- $\gamma$ -inducing factor (IGIF) that directly stimulates the production of IFN- $\gamma$ , resulting in the activation of cellular proliferation and differentiation in T cells and NK cells. The uses of IL-18 as monotherapy against cancer have been shown to be effective in the preclinical models.

The anti-tumor effects of recombinant IL-18 (rIL-18) were observed in murine melanoma (CL8-1) (Osaki et al., 1998). Furthermore, *in vivo* study of anti-tumor effects of rIL-18 using Fas-FasL deficient mice were investigated (Hashimoto et al., 1999). Anti-cancer properties of rIL-18 were abrogated in FasL-deficient mice due to the growth of tumor volume. These results indicate that IL-18 has potent anti-tumor properties by promoting cytotoxic activities in T cells and NK cells through IFN- $\gamma$  production and Fas-FasL pathway as well. In clinically, recombinant human IL-18 (rhIL-18) administered by intravenous (IV) infusion to patients with advanced cancer have been evaluated.

The cytokines are capable of potentiating anti-tumor immune responses and recruiting immune effector cells into tumor sites leading to tumor regression in advanced cancers (Robertson et al., 2006). On the other hand, phase II clinical trial of rhIL-18 in untreated metastatic melanoma patients demonstrated that the patients

showed a low overall response rate (ORR) when treated with rhIL-18 IV infusion (0.01, 0.1, and 1 mg/kg/day) in each groups (Tarhini et al., 2009). These results implied that IL-18 monotherapy has shown to be of limited clinical efficacy. Interestingly, study using BALB/c mice with metastasis melanoma, colon cancer, and breast cancer informed revealed that IL-18 synergistically enhanced anti-tumor activities of immune checkpoint inhibitors IL-18 provided a synergistic therapeutic effect with immune checkpoint therapy as a combinatorial approach to improve cancer immunotherapy (Ma et al., 2016).

The anti-tumor effects of intra-tumoral production of IL-18 was also investigated by TCR-engineered T cells in mouse melanoma model (Kunert et al., 2017). They demonstrated that engineered T cells with a melanoma specific TCR and IL-18 expression showed elevated levels of IFN- $\gamma$  and TNF- $\alpha$  in plasma. In addition, the secreted IL-18 provided the accumulation of CD8<sup>+</sup> TILs within tumor sites, reduced tumor progression and improved survival rate in melanoma-bearing mice. Additionally, IL-18 is capable of synergizing with IL-12 for the induction of IFN- $\gamma$  production. Survival rate and prognosis in metastatic melanoma patients could be improved by treating patients with the co-administration of IL-12 and IL-18. The synergistic effect of IL-12 and IL-18 includes the activation of JAK2 and Tyk pathways, and STAT4 phosphorylation that stimulate IFN- $\gamma$  gene expression. Likewise, the activation of MAPK pathway by IL-18 also provided the stabilization of IFN- $\gamma$  mRNA leads to the induction of IFN- $\gamma$  production of NK cells (Martinović et al., 2015).

IL-18 can inhibit malignant progression and metastasis but also significantly boost both innate and adaptive immune response on the anti-tumor activity as a coordinator of the immune system as shown in Table 1.

**Table 1. Anti-tumor properties of IL-18 in preclinical models.**

<b>Types of cancer</b>	<b>Major findings</b>	<b>Ref.</b>
B16 melanoma	IL-18 stimulates the anti-cancer response by promoting NK cell functions with the synergistic effect of $\alpha$ -galactosylceramide lead to a decrease in the number of pulmonary metastatic foci.	Nishio et al., 2018
Prostate carcinoma	IL-18 inhibits the growth of subcutaneous and orthopic prostate carcinomas through the induction of anti-tumor effects in both innate and adaptive immune response.	Tse et al., 2011
Human B cell lymphoma xenograft	The combination of IL-18 and mAbs immunotherapy shows the synergistic effects against tumor progression by promoting the production of IFN- $\gamma$ and inducing ADCC in human B cell lymphoma xenograft model.	Srivastava et al., 2013
SCK mammary carcinoma	IL-18 shows synergistic activity with IL-12 to inhibit SCK tumor progression and angiogenesis in murine models	Coughlin et al., 1998

The binding modes of IL-18 and IL-18 receptor (IL-18R) show the crucial roles to the biological function of IL-18. In addition, another important ability of this cytokine is promoting the anticancer effects (Akira, 2000; Dinarello, 2013) against cancer cells through various mechanisms including: (1) production of IFN- $\gamma$  and other immunomodulatory cytokines, (2) activation of immune effector cells, such as NK cells, CD4<sup>+</sup> T cells, and CD8<sup>+</sup> T cells, (3) upregulation of Fas ligand expression on NK cells, resulting in the induction of apoptosis in tumors, and (4) inhibition of the gene expression of the proangiogenic factors, for example, VEGF, CXCL2, and intercellular adhesion molecule-1 (ICAM-1).

The crystal structure (Tsutsumi et al., 2014) revealed that binding sites of IL-18 are composed of two parts. The first part of binding site interacts specifically with IL-18R $\alpha$  are site I and site II, and site III are important for IL-18R $\beta$  receptor binding. Some amino acid residues including Glu-6, Lys-53, and Ser-55 that are located on the binding interface between IL-18 and the specific receptor importantly serves as binding residues to forming a complex on the surface of the receptor (Kato et al., 2003). The binding site I consists of Arg13, Asp17, Met33, Asp35 and Asp132. The site II includes Lys4, Leu5, Lys8, Arg58, Met60 and Arg104. Likewise, the contact sites of IL-18R $\beta$  are composed of Lys79, Lys84 and Asp98. In addition to the receptor-binding residues, some amino acids are also significant in the binding ability and biological function of IL-18, such as Glu6, Lys53 and Thr63 as shown in Figure 1.

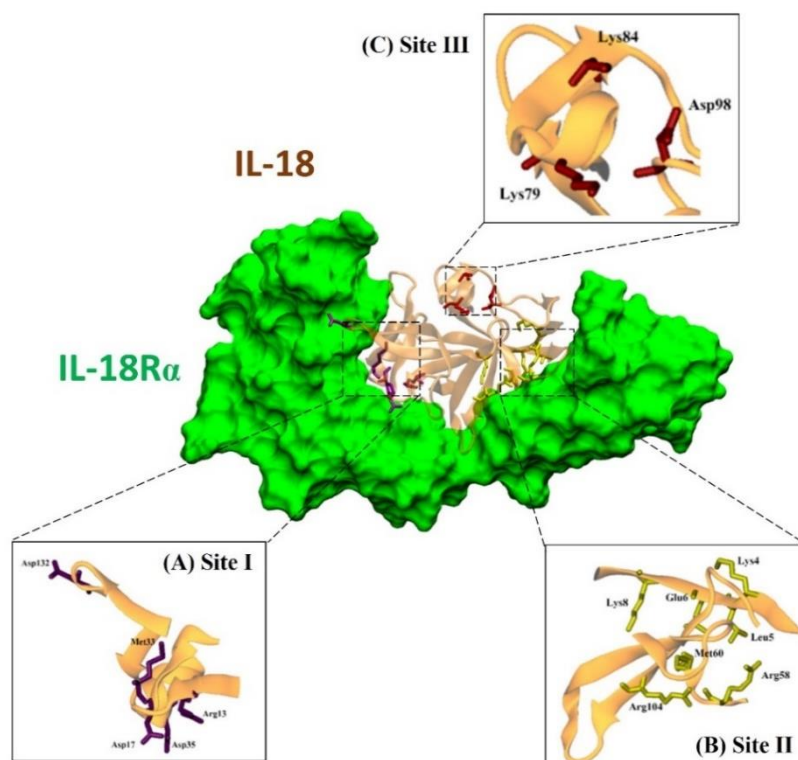


**Figure 1. Structure of IL-18 and IL-18R $\alpha$  binding.** (A) Amino acids in the binding interface of IL-18 and IL18R $\alpha$  as site I. (B) The binding residues in receptor binding site II (C) the key residues in site III of IL18 and its receptor, IL18R $\beta$ . The IL-18 and IL-18R $\alpha$  structures were depicted in orange and green. The complex structure was taken from PDB structure 3WO3.

The modification of amino acids on the binding sites of IL-18 through molecular cloning and mutagenesis techniques can enhance biological activity regarding the induction of IFN- $\gamma$  production in tumor immunotherapy (Saetang et al., 2016). Interestingly, the amino acid alterations on Glu6 of IL-18 by two mutations, E6A and E6K have shown ability to induce the IFN- $\gamma$  production in NK cell lines. (Saetang et al., 2016; Kim et al., 2001) Targeting the binding sites and amino acid residues of IL-18 is an attractive strategy to improve the activity of this cytokine. However, *in vitro* study is enormously expensive, time-consuming and challenging to produce the recombinant engineered proteins effectively.

Nowadays, computational-based protein design facilitates the discovery and development of novel protein with reduced cost-related and time-spent on the workbench. Therefore, we apply this computational technique to design and predict the biological activity enhancement of IL-18 so that the novel potential IL-18 will be obtained for immunotherapy alternative.

### **1.3 Strategy to improve the biological of IL-18 by using site-directed mutagenesis**

Previous research covered two main goals for the efficacy improvement in which mutational approaches (as shown in Table 2.) have been employed: generating protein stability and enhancing protein biological activity.

A highly stable IL-18 mutant with substitution of cysteine by serine (C38S, C68S, C76S, and C127S) in amino acid sequences of IL-18 based on a ligand-receptor complex structure was reported (Yamamoto et al., 2004). These mutants showed higher stability to oxidative conditions while remaining the biological activities. Furthermore, the engineered IL-18 with the replacement of valine at the 11<sup>th</sup> amino acid sequence to isoleucine (V11I) showed ability to stabilize the protein structure and facilitate proper folding that related to the relative expression level in protein expression experiment (Underwood et al., 2006).

Glu-6, negatively charged amino acid which is located on the same surface area of the residues in site II. The structure of human IL-18 bound to its receptors have been demonstrated by Kato et al. (2014). The Glu-6 is the surface-exposed residue that are involved in direct binding to IL-18R $\alpha$  on the binding interface of IL-

18, suggesting the importance of Glu-6 for triggering the biological functions of this cytokine. The single point mutation of Glu-6 to Ala (E6A) showed 2-fold increase in biological activity when compared with IL-18 wild type (Kim et al., 2001). Interestingly, the combination of E6A and K53A mutation provided 4-fold higher activity than IL-18 wild type. Moreover, the activity of E6K mutant was more effective about 2 times higher than IL-18 wild type.

**Table 2. Biological activity of the mutants compared with IL-18 wild type.**

<b>Mutation</b>	<b>Biological activity compared with IL-18 wild type (fold)</b>	<b>Ref.</b>
<b>wild type</b>	1x	-
<b>E6A</b>	1-2.6x	Kim et al., 2001
<b>E6K</b>	9.3x	Saetang et al., 2016 and Kim et al., 2002
<b>E6del</b>	Decreased activity	Kim et al., 2002
<b>S10T</b> <b>V11I</b>	Improved stability	Underwood et al., 2006
<b>K53E</b>	Decreased activity	Kim et al., 2002
<b>T63A</b>	3.9x	Saetang et al., 2016 and Underwood et al., 2006
<b>E6A+K53A</b>	>4x	Kim et al., 2001
<b>E6K+T63A</b>	16x	Saetang et al., 2016
<b>S10T+T63A</b>	1.7x	Underwood et al., 2006
<b>V11I+T63A</b>	2.6x	Underwood et al., 2006
<b>S10T+D17N+T63A</b>	2.2x	Underwood et al., 2006
<b>C38S/C68S/C76S/C127S</b>	Improved stability	Yamamoto et al., 2004

Recently, novel IL-18 mutants with improved biological activity have been reported by Saetang et al. (2016). The double mutation E6K plus T63A exhibited 16-fold enhanced interferon- $\gamma$  induction activity compared to wild type (Saetang et al., 2016). In the same way, the deletion of Glu-6 (E6del) generally impaired the

biological function of IL-18 to stimulate the IFN- $\gamma$  production in NK cells. These findings suggested the importance of Glu-6 as a critical amino acid residue for biological activity of IL-18.

#### **1.4 Computational approaches for designing therapeutic proteins and peptides**

Computational approaches have been considered as an attractive strategy for designing and engineering therapeutic proteins during the past two decades. The use of computational methods in protein design provides new insights into the relationship between protein sequence, structure, and function at the atomic level which can integrate with protein engineering to create/engineer therapeutic proteins with improved modes of action, such as activities, stabilities, and specificities (Kim et al., 2002). The techniques of computationally designing proteins are involved in two main approaches including template-based design methods and *de novo* protein design.

Firstly, template-based design methods, one of the computational protein design approaches that utilize the known sequences or pre-existing three-dimensional (3D) structure of proteins in protein databases as a template for designing and creating new proteins. Secondly, the idea of protein can be designed from scratch termed *de novo* protein design, this approach relies on the principle that proteins fold into their lowest free-energy states; therefore, finding an amino acid sequence that fold to the lowest energy state are required for designing a new potential protein structure (Hwang & Park, 2008; Childers & Daggett, 2017).

##### **1.4.1 Template-based design**

The idea of protein design using template-based modeling approach relies on the principle that homologous proteins of similar sequences should provide similar structure and protein features. This method has been used to construct modified proteins by aligning and predicting the sequence and structure feature of the target proteins with the experimentally identified complex structures in the protein data bank (PDB). To achieve a new protein, computational approaches for protein design via template-based modeling are driven by three general steps (Figure 2) (Silva et al., 2019; Szilagyi & Zhang, 2014).

Initially, seeking for the suitable structures (templates) that related to the target protein to be constructed based on the alignment of amino acid sequences and structure feature of target protein with database information, and subsequently the best template of the highest score is chosen as the structural model of the target protein. Secondly, modifying the selected template to improve the potential of target protein including structural stability or binding affinity based on the understanding of binding interface, structural recognition and protein-protein interactions through the modified structure template at atomic level. Finally, the modified structure of target protein is required to be optimized by energy minimization using web server or bioinformatics software that remove unfavorable contacts. Consequently, the energy-minimized structure should be rather close to the native conformation, resulting in achieving the structural model for the design of therapeutic protein (Szilagyí & Zhang, 2014; Roy et al., 2017).

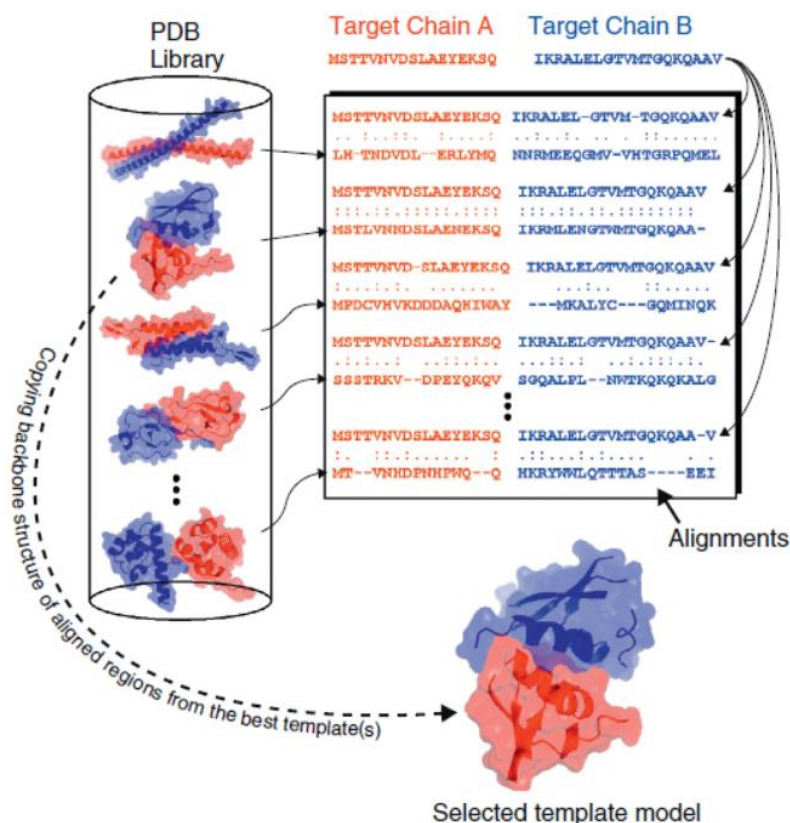


**Figure 2. Overview of template-based structure modeling protein design.**

### 1.4.2 *De novo* protein design

*De novo* protein design, the generation of new proteins from scratch, has emerged as a promising computational approach for constructing the novel proteins with non-natural amino acid sequence and structure that possess desired biological functions (Richardson et al., 1989). The idea of *de novo* protein design relies on Anfinsen's experiment that proteins fold to their global free energy minimum. According to this principle, the researchers compute amino acid sequences predicted to fold into proteins with new structures and functions, produce synthetic genes encoding these sequences, and characterize them experimentally (Huang et al., 2016).

The general sequential steps of *de novo* computational protein design include: (1) defining of the target protein structure or topology based on secondary structures, pairings, lengths, sequence-independent rules, and geometric constraints; (2) generating appropriate protein backbones that best suit the target using backbone building computational methods, such as kinematic closure, fragment assembly, parametric, and structure extension with native-substructure graphs (SEWING); (3) finding and designing the amino acid sequences or side chain that minimize the energy function on a fixed protein backbone; (4) evaluating the sequence-structure compatibility of the designed protein through fragment-based local compatibility, folding energy landscape, or local tertiary structure motifs (TERMs) score; and, finally, constructing and validating the top-ranked of the *de novo* designed protein using experimental methods including site-directed mutagenesis or directed-evolution (Marcos & Silva, 2018). The overview workflow of *de novo* computational protein design and their therapeutic applications as shown in Figure 3 and Table 3.

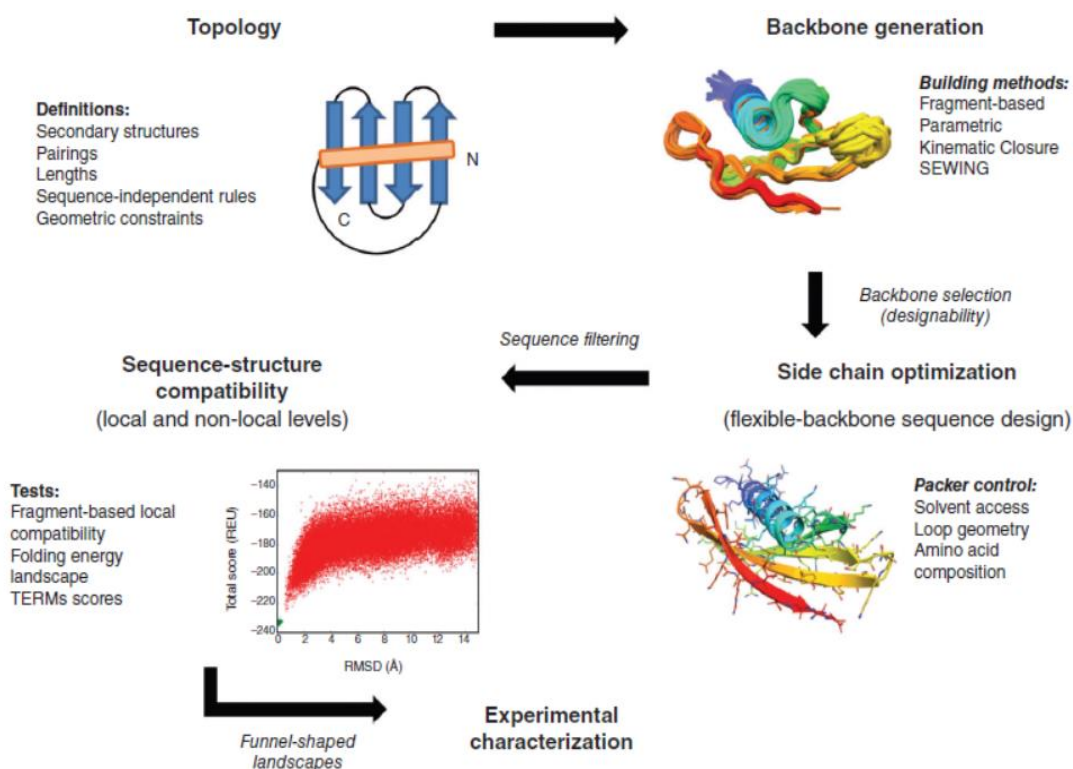


**Figure 3. Workflow of *de novo* computational protein design.**

Nowadays, computational design and *in silico* screening generate novel engineered proteins with reduced cost-related and time-spent on the workbench. Therefore, we apply the computational approaches and protein engineering to examine the effects of each mutation on the biological activity of IL-18 so that it will be provided a basis and advantages as a structure-guided protein design for further exploitation of cytokine-mediated immunotherapy.

**Table 3. Summary of recent computationally designed proteins and peptides and their therapeutic applications.**

Target	Methodology		Significance	Ref.
	Computational	Experimental		
CRIP1	<i>De novo</i> design via Eris, Insight II, ZDOCK	Directed-evolution	Ligand binding leads to an approximately 10-28 fold increase in binding affinity	Hao et al., 2008
Influenza Hemagglutinin (HA) Protein	Rosetta Design	Directed-evolution	The designed proteins showed ability to bind multiple HA strains that could prevent viral infection	Fleishman et al., 2011
Myxoma Virus (MV) proteins	Resonant Recognition Model (RRM)	Peptide synthesis	Short bioactive peptide analogue (RRM-MV) induced cellular cytotoxic effect on B16F0 mouse melanoma cells	Istivan et al., 2019
IL-2	Rosetta Design	Site-directed mutagenesis	Designed neoleukin-2 binds IL-2R $\beta$ with high affinity and provides therapeutic activity in melanoma and colon cancer mouse models	Silva et al., 2019
Nitric oxide reductase (NOR)	VMD software, Molecular dynamics simulation via NAMD	Site-directed mutagenesis	The successful structural and functional model of NOR	Natasha et al., 2009

### **1.5 Objectives**

1. To identify and screen the potential mutation increasing the activity of IL-18 using structure-based energy calculation approaches.
2. To investigate the impacts of the amino acid alteration on the conformational stability and dynamic behavior of IL-18 structure using molecular dynamics simulation technique.

## CHAPTER 2

### RESEARCH METHODOLOGY

#### 2.1 Schematic overview

Since the biological activity of IL-18 required the specific binding to IL-18 receptors, the aim of our study was to design mutations increasing the affinity of IL-18 towards its receptor through computational structure-based energy calculation and protein design. The first step involved analysis of per-residue free energy decomposition to identify the unfavorable residues at the binding interface IL-18. Furthermore, *in silico* saturation mutagenesis approach is used to screen and design the energetically favorable mutations of IL-18 with improved activity by introducing all possible single site amino acid substitution to the selected unfavorable residues.

The mutated structures were computed for their free energy changes ( $\Delta\Delta G$ ) upon mutations in order to investigate the impact of mutation on the binding affinity and stability of protein. The candidate favorable mutation was subjected to perform molecular dynamic (MD) simulation to evaluate dynamic behavior and atomistic insight into the structure of protein. Therefore, our computational approach is able to provide a basis and advantages as a structure-guided protein design for further exploitation of cytokine-mediated immunotherapy. The overview of this study as shown in Figure 4.

#### 2.2 Computational resources

All computation and analysis in this study were performed on computer Dell, Cluster in Ubuntu 16.04 LTS Linux systems, NVIDIA Quadro P5000, Intel® Core™ i7 7700K CPU/4.20 GHz. located at Department of Biomedical Sciences, Faculty of Medicine, Prince of Songkla University, Hat Yai, Songkhla 90112, Thailand.

Software products used in the computational analysis and protein design were Visual Molecular Dynamics (VMD) 1.9.3 (Humphrey et al., 1996), FoldX 5.0

(Delgado et al., 2019), and Amber16 Package (Case et al, 2015). Other bioinformatics webtools used in this study were RCSB Protein Data Bank (<http://www.rcsb.org>), PROPKA (<http://propka.org>) (Sondergaard et al., 2017), and pyDockEneRes (<https://life.bsc.es/pid/pydockeneres>) (Romero-Durana et al., 2020).

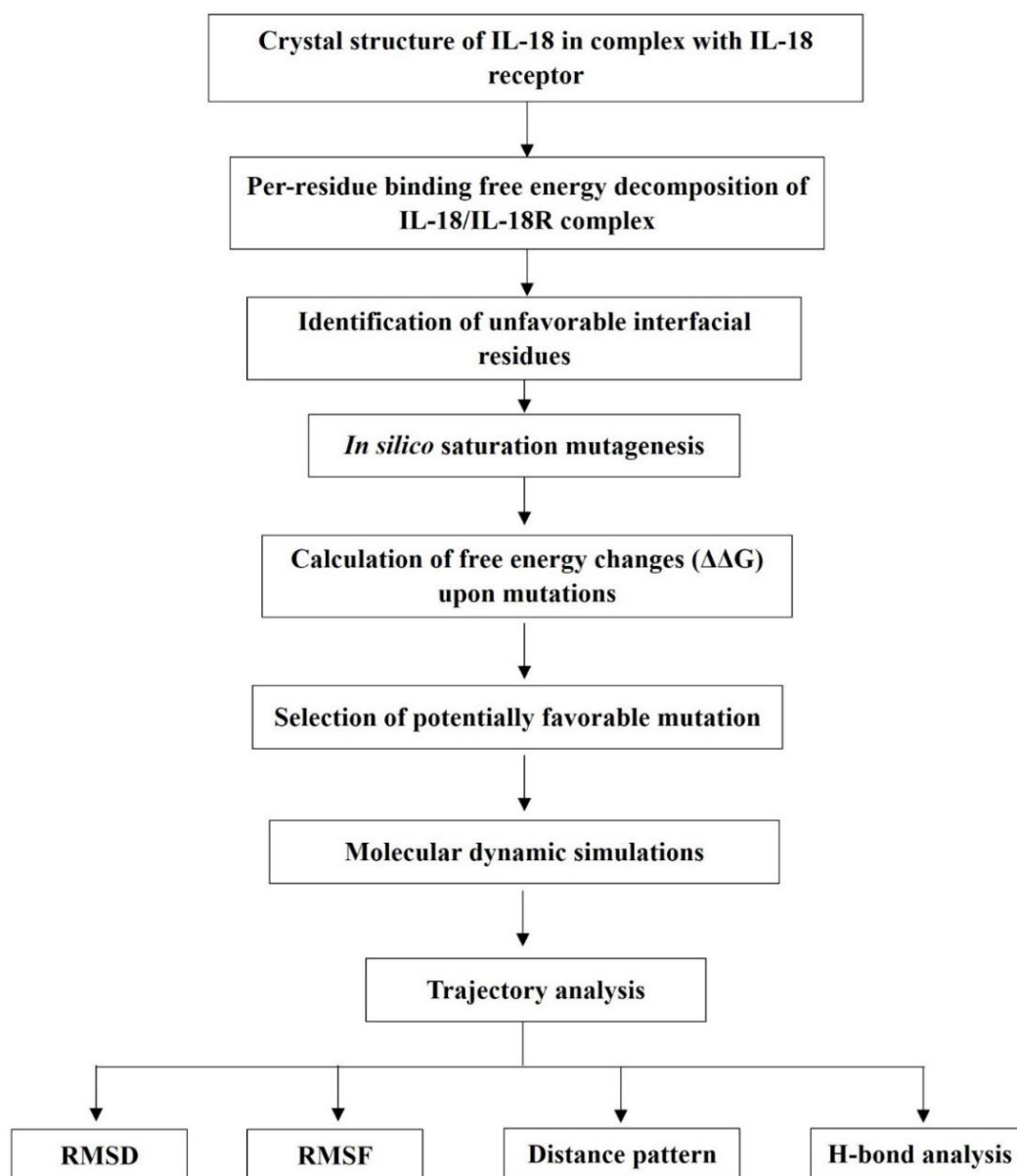


**Figure 4. Study overview shows a strategy to acquire the effective mutation candidate of IL-18.** The screening and design for mutation, which could enhance biological activity, was performed using the integration of computational structure-based energy calculation and molecular dynamic simulations.

## **2.3 *In-silico* mutagenesis and energy decomposition**

### **2.3.1 Structure preparation**

An X-Ray structure of human IL-18 in complex with IL-18 receptor alpha, with a resolution of 3.10 Å (PDB entry: 3WO3) (Tsutsumi et al., 2014) was downloaded from Research Collaboratory for Structural Bioinformatics (RCSB) Protein Data Bank in PDB file format (\*.pdb). The solvent molecules in the co-crystallized protein structure were removed. The chain A and chain B were selected for further analysis. The protein structure visualization and rendering were performed using Visual Molecular Dynamics (VMD) version 1.9.3, in order to determine the information about atom types, numbering of atoms, masses, charges, bonds, angles and dihedrals of the complex structure.

Prior to the generation of mutated structure, the 3WO3 structure must be subjected to optimization procedure using RepairPDB command in FoldX5, to remove steric hindrances and unfavorable high-energy conformations. To generate the mutant protein, the selected amino acid of the repaired structure was modified into the new residues using the BuildModel function. The numberOfRuns option was set to 5 for ensuring the minimal energy conformation because some residues can have the different rotameric conformations. All other parameters were set to default, including pH (7), ionic strength (0.05 M), vdWDesign (2), and temperature (310 K).

### **2.3.2 Energy decomposition**

The contribution of individual residue to the binding energy of IL-18 towards its receptor was calculated using per-residue energy decomposition ( $\Delta G_{\text{residue}}$ ). The crystal structure of human IL-18 in complex with receptor was decomposed by Fast Fourier Transform (FFT)-based docking method implemented in pyDockEneRes server.

### **2.3.3 *In-silico* mutagenesis**

The residue of interest of IL-18 structure was mutated to all 19 possible amino acids using BuildModel module in FoldX algorithm. To validate the computational predictions, the reported mutations with *in vitro* activities were also generated using

the BuildModel as described above. The 17 known mutations, related function impairment or IL-18 activity improvement (Kato et al., 2003; Saetang et al., 2016), were considered for method validation, namely including K4A, L5A, K8A, D17A, R13A, M33A, D35A, R58A, M60A, R104A, D132A, K79A, K84A, D98A, E6K, and E6K+T63A.

### **2.3.4 Analysis of relative binding free energy change upon mutation**

AnalyzeComplex function of FoldX software was used to calculate the free-energy change after IL-18 was mutated with respect to IL18 receptor (IL18R). Three types of free energy changes ( $\Delta\Delta G$ ,  $\Delta G_{\text{mutant}} - \Delta G_{\text{wild-type}}$ ) were computed. The difference in binding free energy ( $\Delta\Delta G$  binding) of IL-18/IL18R complex determined the change of the interaction. The difference in folding free energy ( $\Delta\Delta G$  folding) of IL-18 estimated the effect of mutations on the stability of the IL-18/IL-18R complex. The difference in free energy folding of free IL-18 ( $\Delta\Delta G$  folding of free IL-18) calculated the sole influence of mutations on the IL-18 stability.

### **2.3.5 Statistical analysis**

Correlation between the relative binding free energy changes upon mutation ( $\Delta\Delta G$ ) of IL-18/IL-18R complex were evaluated using Pearson's correlation and simple linear regression. A  $p$  value  $< 0.01$  and  $0.05$  were considered statistically significant. All statistical analyses were performed using Libre Office Calc 5 in Ubuntu 16.04 LTS Linux systems.

## **2.4 Molecular dynamics (MD) simulation**

### **2.4.1 System preparation**

MD simulations were performed in order to mimic an *in vivo* condition and investigated for conformational dynamic behaviors. All MD simulations were done using AMBER 16 software (Case et al, 2015). The crystal structure of human IL-18, PDB code 3WO3, and designed IL-18 mutants from 2.3 were chosen for the initial structures for preparing MD simulation. The protonation state of the ionizable amino acids (Lys, Arg, His, Asp, and Glu) were calculated using PROPKA webtools

(Sondergaard et al., 2017) at pH 7. All missing hydrogen atoms of protein structure were added using LEaP module in AMBER16 package. Each system was neutralized by the counter ions and solvated in a concentration of  $0.15 \text{ mol dm}^{-3}$  sodium chloride (NaCl) using TIP3P (Jorgensen et al., 1983) water box with extended distance of  $14 \text{ \AA}$  from the protein surface. Finally the system contained approximately 11400 water molecules and 30 NaCl pairs excluding counter ions. The system was then saved into AMBER parameter topology (.prmtop) file along with an AMBER7 restart file (.rst7) for energy minimization.

#### **2.4.2 Energy minimization**

The energy minimization ( $\text{imin} = 1$ ) was carried out by the steepest descent and conjugate gradient methods for 1,000 and 1,000 steps, respectively to remove bad van der Waals contact with a cutoff  $16 \text{ \AA}$  ( $\text{cut} = 16$ ). The energy minimization methods were implemented in the PMEMD.cuda module (Darden et al., 1993) under a periodic boundary condition ( $\text{ntb} = 1$ ). The final minimized coordinate was obtained in a form of Amber7 restart file (.rst7) to later continue MD simulation. The input file was written in the appendix section.

#### **2.4.2 Canonical (NVT) ensemble**

The minimized protein structure was subjected to perform MD simulation ( $\text{imin} = 0$ ) in 2-nanosecond-isothermal ensemble (NVT) simulation with 1fs-time step, using force constants of 200, 100, 50, 25, and 10 kcal/mol, respectively. The harmonic restrained potential was applied into the protein residue (Residue 1 to 156). Each force constant lasted for 400 picoseconds (ps). The temperature of 310 K ( $37^\circ\text{C}$ ) was controlled with Langevin dynamics ( $\text{ntt} = 3$ ) (Uberuaga et al., 2004). The nonbonded and electrostatic interactions were handled with a cutoff of  $16 \text{ \AA}$  using Particle Mesh Ewald (PME) summation (Darden, York, and Pedersen, 1993). The NVT ensemble was carried out with the PMEMD.cuda module under a periodic boundary condition ( $\text{ntb} = 1$ ). The hydrogen-connected bond (H-X) was restrained using SHAKE algorithm ( $\text{ntc} = 2$ ) (Ryckaert et al., 1977). The input file was written in the appendix section.

### 2.4.3 Isobaric-Isothermal (NPT) ensemble

Then, the system was simulated under the periodic boundary condition (ntb = 1) with the isothermal-isobaric (NPT) ensemble of 310 K (temp0 = 310) and 1 atm (1.013 bar) (pres0=1.013) until reaching 150 nanoseconds (ns) (2500 snapshots). The temperature and pressure were regulated using a weak-coupling (Berendsen) algorithm (ntt = 1, ntp = 1) (Berendsen et al., 1984). The hydrogen-connected bond was restrained using SHAKE algorithm (ntc = 2.). The input file was written in the appendix section. The first 90 ns-simulation (1500 snapshots) was omitted and the MD trajectory was extracted from the last 60 ns (1000 snapshots) for a structural analysis using cpptraj module in AMBER16. The structure visualization was done using VMD software

## 2.5 Trajectory analysis

### 2.5.1 Root mean square deviation (RMSD)

Root mean square deviation (RMSD) is the quantitative measure of the average distance between the atoms (especially the backbone atoms) of the protein structure from MD trajectory and its reference crystal structure. RMSD was used as an estimator of similarity between two protein structures.

In addition, RMSD was also considered for energy convergence (stability) of MD simulation. RMSD value is expressed in a unit of angstrom (Å) and calculated by

$$\text{RMSD}(t) = \sqrt{\frac{1}{N_{\text{atoms}}} \sum_{i=1}^{N_{\text{atoms}}} (\mathbf{x}_i(t) - \mathbf{x}_i(t_0))^2},$$

where  $N_{\text{atoms}}$  is the number of atoms,  $\mathbf{x}_i(t)$  is the  $i$ -th atom coordinate at time  $t$ . Generally, the acceptable range of the RMSD value is less than 3 Å that indicates high similarity to the native structure.

### 2.5.2 Root mean square fluctuation (RMSF)

Root mean square fluctuation (RMSF) is a measure of spatial fluctuations or flexibility of atoms over their average motion during MD simulation. RMSF value is expressed in a unit of angstrom ( $\text{\AA}$ ) unit. Their definition are

$$\text{RMSF}_i = \left[ \frac{1}{T} \sum_{t_j=1}^T |\mathbf{r}_i(t_j) - \mathbf{r}_i^{\text{ref}}|^2 \right]^{1/2}$$

where  $T$  is the trajectory time of MD simulation,  $\mathbf{r}_i(t_j)$  is the atomic position  $i$  at time  $t$ , and  $\mathbf{r}_i^{\text{ref}}$  is the reference position of atom  $i$

### 2.5.3 Distance pattern

The distance pattern was used to determine conformational comparison between mutated IL-18 and native IL-18. The distance pattern was obtained from an average distance of the geometric center of backbone atoms (N, C, CA, and O atoms) in each amino acid to an origin point (0,0,0). The average distance in a unit of  $\text{\AA}$  was taken from 1000 MD snapshots. The difference in average distance of corresponding amino acids between native and mutated IL-18 structures indicated the different conformation.

### 2.5.4 Hydrogen bonding analysis

The hydrogen bond was analyzed from 1000 snapshots of MD trajectory. Hydrogen bond interactions were calculated using two criteria: (1) distance between the hydrogen donor (HD) and acceptor (HA) of not more than  $3.5 \text{\AA}$ , and (2) HD-H $\cdots$ HA angle of at least  $150^\circ$  (Nutho et al., 2020).

## CHAPTER 3

### RESULT AND DISCUSSION

#### 3.1 Preliminary design of IL-18 using interaction-based point mutation

The mutant model of the selected residue was mutated *in silico* using the PyMOL mutagenesis wizard (Rigsby & Parker, 2016). IL-18 wild-type and two mutation models (E6K and M33Q) with experimental results from the previous study (Saetang et al., 2016) were considered as a control group to validate the computational method. All protein structure visualization and rendering were performed using Visual Molecular Dynamics (VMD) version 1.9.3. Protein docking was performed using ClusPro 2.0 server (Kozakov et al., 2017). The complex structures were further submitted to PRODIGY webtools (Xue et al., 2016) to estimate the binding affinity of the complexes of IL-18/IL-18 receptor in terms of binding free energy ( $\Delta G$ ) in kcal/mol and dissociation constant ( $K_d$ ) in molar units.

##### 3.1.1 *In silico* design of IL-18

After analyzing the interaction between IL-18 and its receptors, Asn41 in site I is surrounded by positively charged amino acid (Arg25 and His27) on the surface of IL-18R $\alpha$ . Asn41 was substituted by Asp to facilitate the binding affinity by using electrostatic forces and surface charge complementarity. As shown in Figure 5. (A) Asn41 directly interacted with positively charged amino acid side chains of IL-18R $\alpha$  through electrostatic interactions. (B) Molecular interaction between the mutated structure, N41D and IL-18R $\alpha$  at site I (white) was shown.

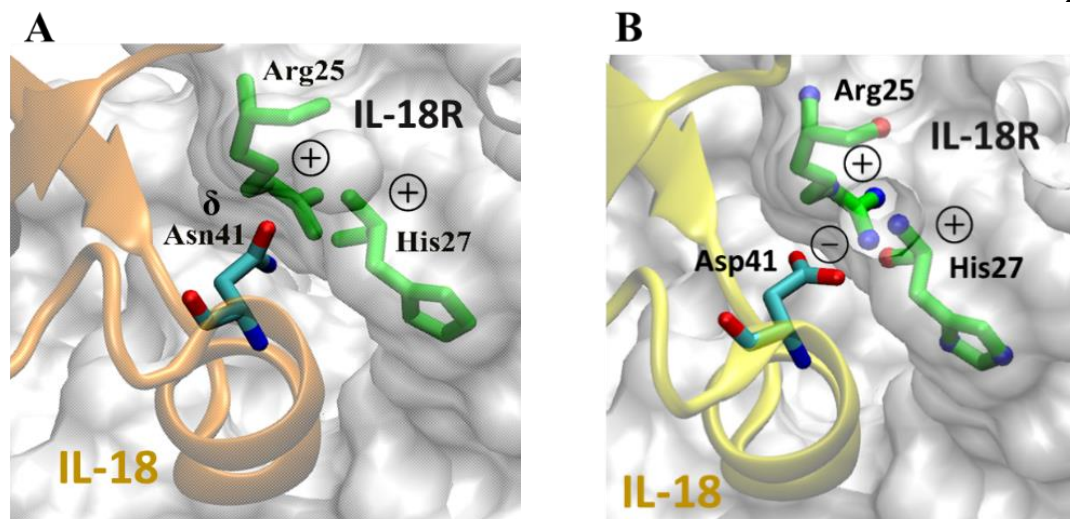


**Figure 5. Structural comparison between IL-18 wild-type (orange) and N41D (yellow) mutant.**

### 3.1.2 Conformational analysis of IL-18 MD trajectory

The wild-type and mutant structures (E6K, M33Q and N41D) showed almost a similar pattern in terms of the RMSD values during a simulation time of 100 ns (Figure 6). The RMSD value below 3 Å was observed from both cases. The stable RMSD was found after a 40 ns simulation with the averaged RMSD values of the wild-type, E6K, M33Q and N41D mutant were 1.63, 1.49, 1.82 and 1.45 Å, respectively. A small variation in the average RMSD values of wild-type and N41D mutant after MD simulations lead to the conclusion that the mutation of Asn-41 to aspartic acid had no effect on the overall conformation and folding of protein.

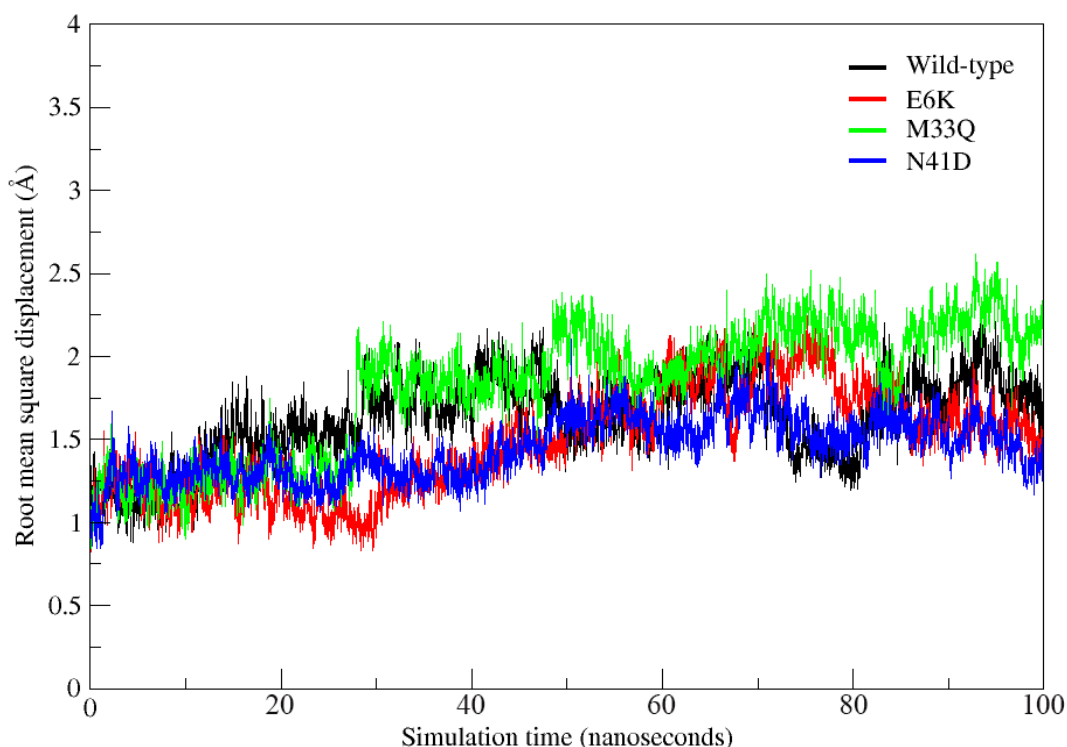


**Figure 6. Root-mean-square deviation (RMSD) from MD simulation of all IL-18 structures in Angstrom units.** Four MD simulations were carried out, namely wild-type (black), E6K (red), M33Q (green), and N41D (blue) respectively.

To determine the effect of the substituted amino acid on the dynamic behavior of the IL-18 residues, the structural flexibility of protein was reported as the RMSF plot in Figure 7. Analysis of fluctuation based on the RMSF values revealed that the flexibility of amino acid residues of the mutants E6K and M33Q have been altered when compared to wild-type, which was in agreement with the activity changes of E6K and M33Q mutant described in the previous experimental study.

Surprisingly, the activity of E6K was increased whereas decreasing in the mutant M33Q. This implies that a higher fluctuation in residues of M33Q mutant may disrupt the binding interaction of IL-18 and its receptors resulting in the activity loss of M33Q, which we discuss in detail in a subsequent section. In this study, the presence of higher RMSF value in the mutant N41D protein was observed when compared to wild-type at residue 90-95 in the loop region connecting  $\beta$ 7 sheet, which plays an important role in the binding interaction of IL-18 and IL-18R $\alpha$  site I. This result suggests that N41D mutation may affect the biological activity of IL-18.

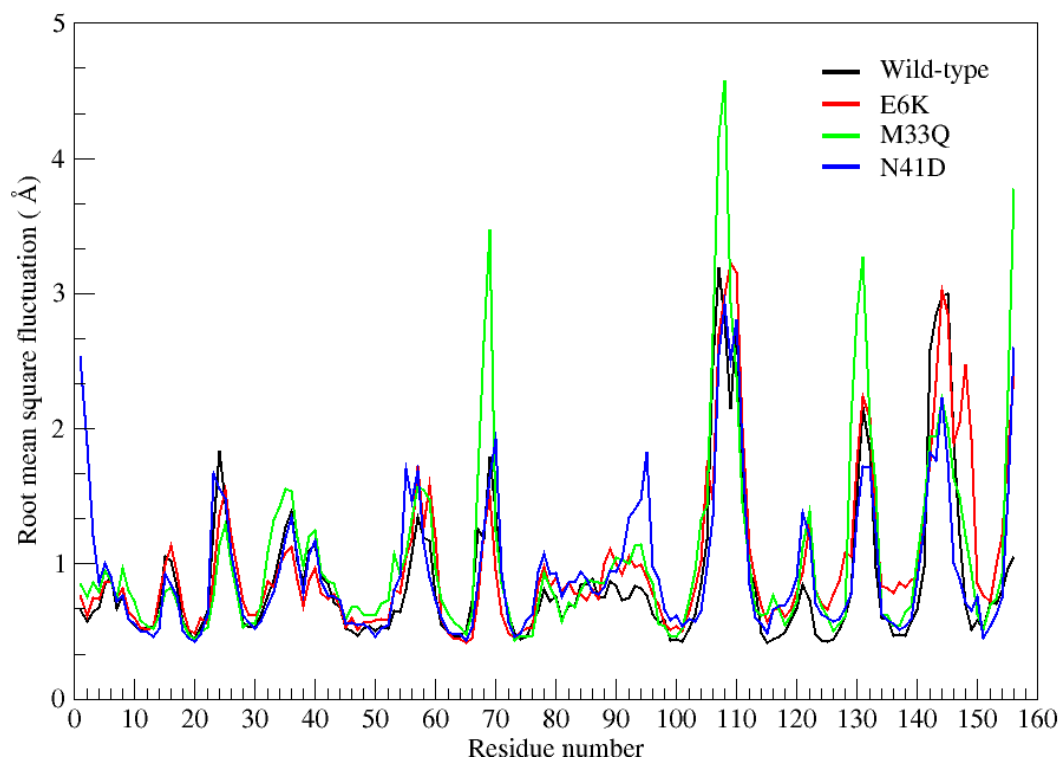


**Figure 7. Root-mean-square fluctuation (RMSF) from MD simulation of all IL-18 structures in Angstrom units.** Four MD simulations were carried out, namely wild-type (black), E6K (red), M33Q (green), and N41D (blue) respectively.

### 3.1.3 Binding affinity evaluation

To evaluate the binding affinity of IL-18 mutant N41D against wild-type and other two control mutants E6K and M33Q. The docking process was conducted by using ClusPro 2.0 server, the binding affinity of protein-protein complexes was determined using PRODIGY server. The predicted value of binding free energy ( $\Delta G$ ) and dissociation constant ( $K_d$ ) of docking results were shown in Table 4.

Our computational study demonstrated that the binding affinity of IL-18 wild-type, E6K, and M33Q mutants in the control group was consistent with their biological activities in the previous experimental study. In this work, the computationally designed IL-18 with N41D mutation showed the strongest binding affinity with  $\Delta G = -15.6$  kcal/mol and better dissociation constant ( $K_d$ ) of  $9.40 \times 10^{-12}$  molar compared to wild-type and E6K mutant (positive control) with lesser affinity -14.1 kcal/mol and -15.4 kcal/mol respectively. These results suggested that the substitution of Asn41 to aspartic acid may improve IL-18 activity by increasing anionicity in N41D.

**Table 4. Predicted binding affinity and biological activity of wild-type and mutant IL-18 structures.**

<b>Mutation</b>	<b>Predicted <math>\Delta G</math> (kcal/mol)</b>	<b>Predicted <math>K_d</math> (M)</b>	<b>Binding affinity</b>	<b>Biological activity<sup>a</sup></b>	<b>Ref.</b>
<i>Control</i>					
Wild-type	-14.1	$1.10 \times 10^{-10}$	Standard	Standard	Saetang et al., 2016
E6K	-15.4	$1.50 \times 10^{-11}$	Increase	Increased activity	Saetang et al., 2016
M33Q	-13.4	$3.90 \times 10^{-10}$	Decrease	Decreased activity	Saetang et al., 2016
N41D	-15.6	$9.40 \times 10^{-12}$	Increase	Predicted increase	-

<sup>a</sup>The biological activity of E6K and M33Q mutants were evaluated experimentally by IFN- $\gamma$  induction assay in NK-92MI cells when compared to IL-18 wild-type (Saetang et al., 2016).

In contrast, the increasing flexibility at the residual level of M33Q mutant (negative control), as mentioned earlier, may result in the loss of the binding interaction between IL-18 and its receptor since the decrease in binding affinity was observed in the M33Q mutant when compared to wild-type. These findings implied that conformational flexibility and binding affinity are responsible for the biological activity of IL-18.

### 3.2. Per-residue decomposition energy

Although the interaction-based was performed and affinity was predicted, the per-residue decomposition energy was introduced to investigate each amino acid contributing to the binding energy. A technique of per-residue binding free energy decomposition can identify the favorable or unfavorable residue on IL-18/IL-18R. The technique can not only easier facilitate the point-by-point amino acid alteration to predict the binding energy, but also quantify the preference of amino acid toward IL-18/IL1-18R interaction.

The per-residue binding free energy relied on Fast Fourier Transform (FFT)-based docking method. The pyDockEneRes server was used to elucidate the important residues of IL-18 that contributed to the receptor binding. The results are shown in Figure 8.

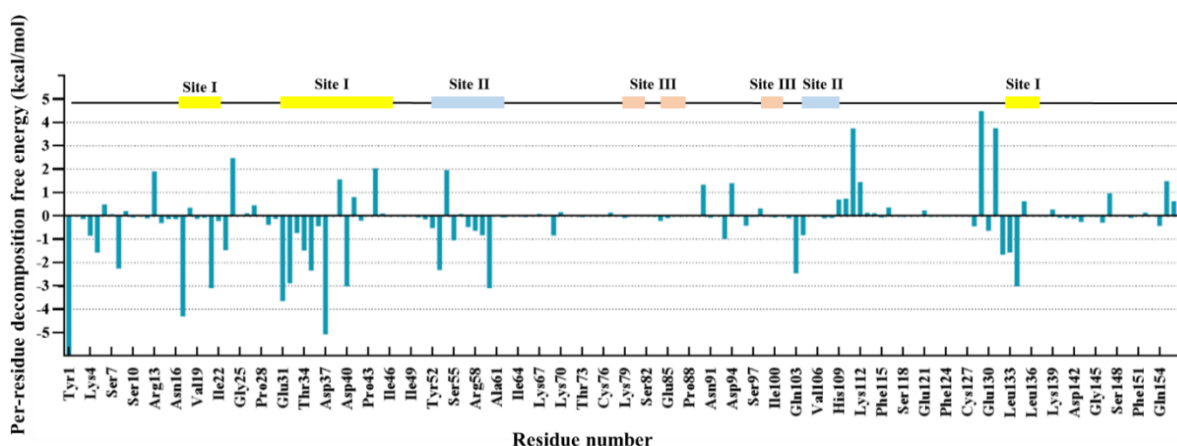


**Figure 8. Decomposition binding free energy of each residue of IL-18.** The key residues involved in the IL18 binding site I, II, and III were colored in yellow, blue, and pink respectively.

### 3.2.1 Contribution analysis of amino acid at IL-18/IL-18R interface

The residues with negative binding free energy contributions are identified as key (favorable) residues responsible for the IL-18/IL-18 receptor interactions at the interface. On the other hand, the residue with positive binding free energy value means the unfavorable interaction residues on the binding interface of IL-18. There were 11 important residues from binding site I and 7 residue from binding site II of IL-18 with binding free energies less than -1 kcal/mol. The 11 residues of binding site I comprise Asp17, Phe21, Glu31, Asp32, Thr34, Asp35, Asp37, Asp40, Asp132, Leu133 and Phe134 whereas the 7 residues of binding site II were Tyr1, Leu5, Lys8, Lys53, Ser55, Met60 and Gln103 (Figure 9).

Seven residues of site I, namely Asp17, Phe21, Asp32, Asp37, Asp40, and Phe134 and one residue of site II, Met60 contributes -3.0 to -5.0 kcal/mol free energy in IL-18/IL-18 receptor complex. Some amino acid residues, such as Met33, Lys93 and Arg104, had the values of the binding free energies approximately -1.0 kcal/mol. These residues contributed favorably to form a ligand-receptor complex by direct binding to the IL-18R $\alpha$ . Similarly, in the binding site III, contributions from Lys79, Lys84 and Asp98 are -0.08, -0.21 and 0.32 kcal/mol respectively in IL18/IL18R $\beta$ . In addition, analysis of the binding free energies based on the electrostatic contribution and the van der Waals energy revealed that the interaction between IL-18 and its receptor is driven by favorable electrostatic and van der Waals contributions that are compensated by unfavorable desolvation contributions (Figure 10).

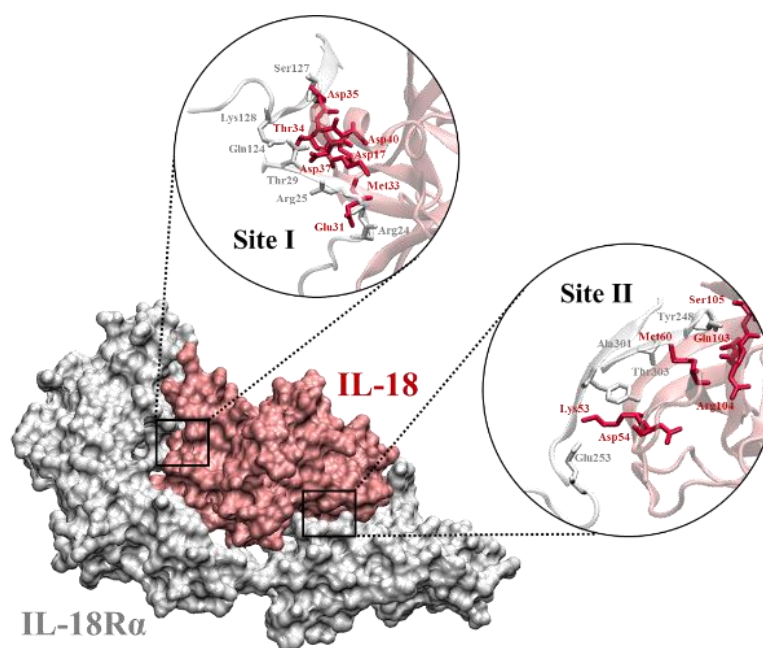


**Figure 9. Schematic representations of the interaction profiles between IL-18/IL-18R $\alpha$  complex.** Interfacial residues of IL-18 and IL-18R $\alpha$  are shown in red and white licorice presentation, respectively.

The results reasonably agreed with the previous experimental mutagenesis studies (Kato et al., 2003; Wei et al., 2014) that the alanine mutation of these residues could abolish the receptor binding and leads to decreased function of the IL-18. Thus, the biological activity of IL-18 required the specific binding to IL-18 receptors, supporting the important of the residues with the favorable energetic contributions at

interface binding play a critical role in IL-18/IL-18R interaction and biological function.

Analysis of per-residue free energy decomposition also revealed unfavorable interface residues. The result exhibited that 11 residues at binding interface of IL-18 were identified as unfavorable residue due to their positive contribution of binding free energies (Figure 11). Four unfavorable residues of binding site I includes Asn41, Arg44, Lys129 and Arg 131, and seven residues of site II consists of Glu6, Asp54, Gln56, Asp110, Asn111, Met113 and Asn155. Since the presence of energetically favorable residues is necessary for IL-18 binding, substituting unfavorable interfacial residues with favorable ones should improve the binding affinity and biological activity of IL-18.

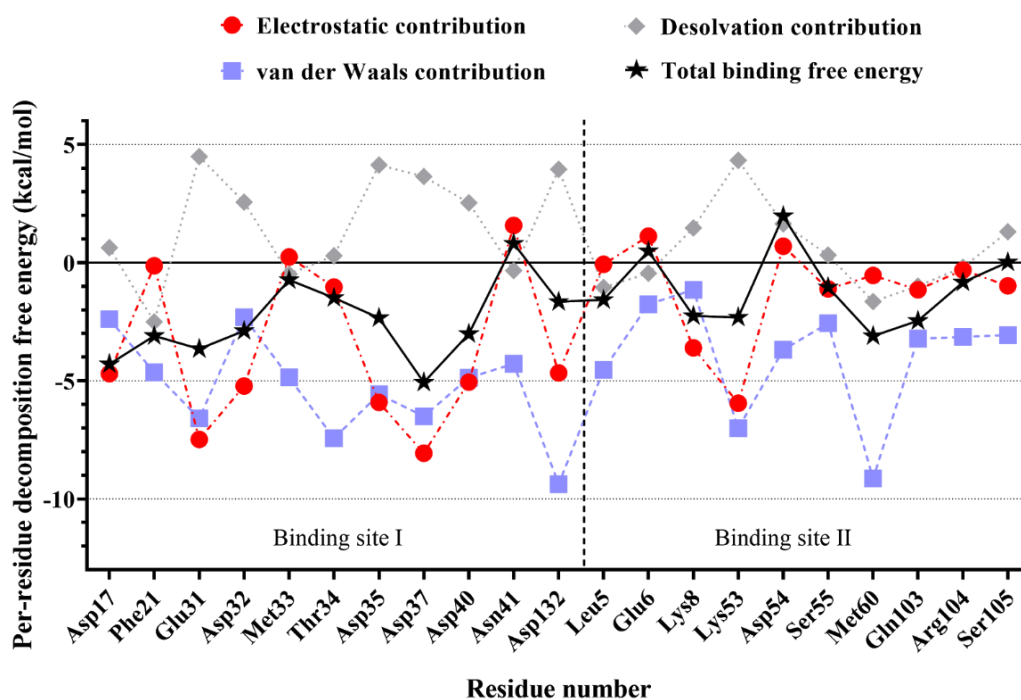


**Figure 10.** Per residue free energy contribution of the key residues in the binding site I and II of IL-18. The energy in kcal/mol was categorized into the electrostatic contribution (red dot), van der Waals contribution (blue dot), desolvation contribution (gray dot) and the total binding free energy (black line).

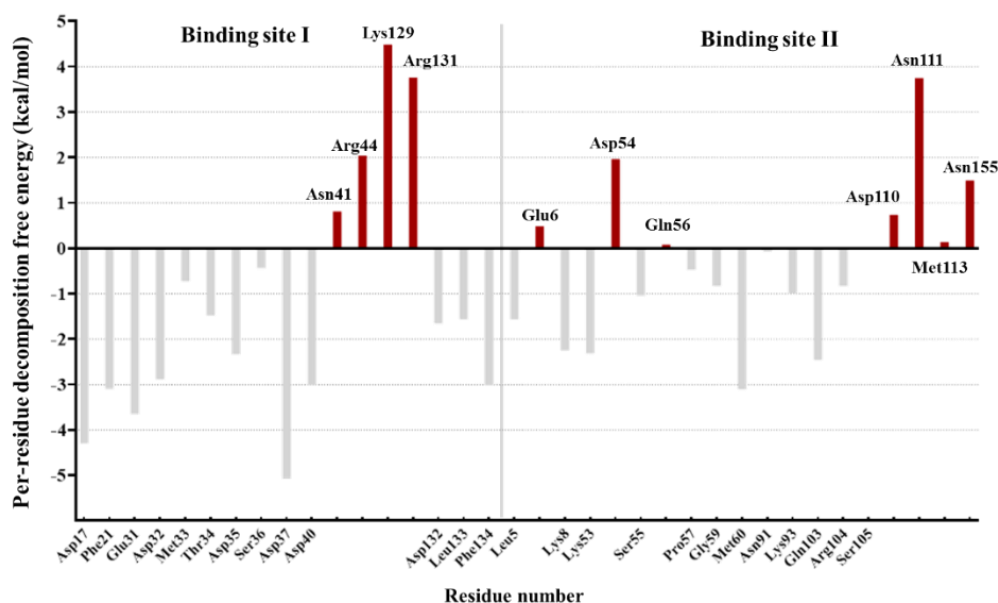


**Figure 11. Per residue free energy contribution of IL-18 in the IL-18/IL-18R interface.** The energy was in kcal/mol. The unfavorable interfacial residues of IL-18 that were selected for optimization were shown in red. The gray bars represented energetically favorable residues of IL-18 in binding site I and II.

### 3.3 Validation of the computational approach

To test the potential reliability of the computational method prior to using this approach to screen favorable amino acid substitution for IL-18 activity enhancement, a total 17 reported mutants in human IL-18 from experiments (Kim et al., 2001; Kato et al., 2003; Saetang et al., 2016) were chosen for a relative binding energy evaluation using FoldX algorithm, namely K4A, L5A, E6A, E6K, K8A, D17A, R13A, M33A, D35A, R58A, M60A, R104A, D132A, K79A, K84A, D98A, and E6A+T63A. These selected IL-18 mutants were in comparison with *in vitro* functional studies as shown in Table 5.

The activity of wild-type was taken as standard (100%) for a calculation of relative activity. Relative activity of mutant was determined by a ratio of a reported activity from mutant IL-18 to an activity from wild-type IL-18.

$$\text{Relative activity} = \frac{\text{In vitro activity of mutant (\%)}}{\text{In vitro activity of wild-type (\%)}}$$

In table 5, the relative free energy ( $\Delta\Delta G$ ) values obtained by FoldX were calculated based on the difference between the energy of mutant ( $\Delta G_{\text{mutant}}$ , in kcal/mol) relative to the energy of wild-type ( $\Delta G_{\text{wild-type}}$ , in kcal/mol) of IL-18.

$$\Delta\Delta G = \Delta G_{\text{mutant}} - \Delta G_{\text{wild-type}}$$

Three types of  $\Delta\Delta G$  value were categorized into

1) “ $\Delta\Delta G$  binding” estimated the change of binding affinity of the wild-type and the mutant variant toward its receptor,

2) “ $\Delta\Delta G$  folding of complex” determined the impact of mutations on the stability of the IL-18/IL-18R complex, and

3) “ $\Delta\Delta G$  folding of free IL-18” investigated the effect of mutations on the stability of isolated IL-18.

$\Delta\Delta G < 0$  (i.e., negative) indicated favorable stability and affinity, and promising mutations, whereas  $\Delta\Delta G > 0$  (i.e., positive) indicated unfavorable stability and affinity toward its receptor.

**Table 5. Comparison of experimental activity and *in silico* predicted relative free energy ( $\Delta\Delta G$ ) in human IL-18.**

<b>Mutation</b>	<b>Relative activity<sup>a</sup></b>	<b><math>\Delta\Delta G</math> binding of IL-18/IL-18R complex</b>	<b><math>\Delta\Delta G</math> folding of IL-18/IL-18R complex</b>	<b><math>\Delta\Delta G</math> folding of IL-18</b>	<b>Ref.</b>
<b>Wild-type</b>	1	0	0	0	Saetang et al., 2016
<b>K4A</b>	0.07	1.46	0.83	0.80	Kato et al., 2003
<b>L5A</b>	0.01	2.86	2.88	1.11	Kato et al., 2003
<b>K8A</b>	0.095	1.3	2.32	1.99	Kato et al., 2003

<sup>a</sup> The biological activity of IL-18 was evaluated experimentally by IFN- $\gamma$  induction assay in NK-92MI cells. Relative activities of mutants were determined by a ratio of a reported activity from mutant IL-18 to an activity from wild-type IL-18.

**Table 5. (Continued)**

<b>Mutation</b>	<b>Relative activity<sup>a</sup></b>	<b><math>\Delta\Delta G</math> binding of IL-18/IL-18R complex</b>	<b><math>\Delta\Delta G</math> folding of IL-18/IL-18R complex</b>	<b><math>\Delta\Delta G</math> folding of IL-18</b>	<b>Ref.</b>
<b>D17A</b>	0.21	1.16	0.95	0.83	Kato et al., 2003
<b>R13A</b>	0.08	0.25	2.95	1.80	Kato et al., 2003
<b>M33A</b>	0.006	0.02	3.66	3.22	Kato et al., 2003
<b>D35A</b>	0.005	6.47	2.42	1.31	Kato et al., 2003
<b>R58A</b>	0.019	0.64	2.24	2.05	Kato et al., 2003
<b>M60A</b>	0.021	0.79	2.48	1.53	Kato et al., 2003
<b>R104A</b>	0.075	0.1	3.28	3.12	Kato et al., 2003
<b>D132A</b>	0.142	1.25	0.82	0.45	Kato et al., 2003
<b>K79A</b>	0.096	1	2.09	2.09	Kato et al., 2003
<b>K84A</b>	0.257	-2.19	0.55	0.55	Kato et al., 2003
<b>D98A</b>	0.167	1.13	-1.15	-1.16	Kato et al., 2003
<b>E6A</b>	2.6	-0.28	0.50	0.56	Kato et al., 2003
<b>E6K</b>	9.3	-1.76	-0.57	-0.27	Saetang et al., 2016
<b>E6K+T63A</b>	16.4	-2.53	0.17	0.48	Saetang et al., 2016

<sup>a</sup> The biological activity of IL-18 was evaluated experimentally by IFN- $\gamma$  induction assay in NK-92MI cells. Relative activities of mutants were determined by a ratio of a reported activity from mutant IL-18 to an activity from wild-type IL-18.

In comparison with experimental data, three types of  $\Delta\Delta G$  value were plotted against the natural logarithm (ln) of % *in vitro* activity. Then, the values were analyzed and interpreted using Pearson's correlation. Pearson correlation coefficient (r) between three types of changes of free energy and experimental activity of each mutant is -0.7019 ( $p=0.0012$ ), -0.7443 ( $p=0.0004$ ) and -0.5770 ( $p=0.0122$ ) for  $\Delta\Delta G_{\text{binding}}$ ,  $\Delta\Delta G_{\text{folding of complex}}$  and  $\Delta\Delta G_{\text{folding of isolated ligand}}$ , as shown in Figure 12 , Figure 13 and Figure 14 , respectively.

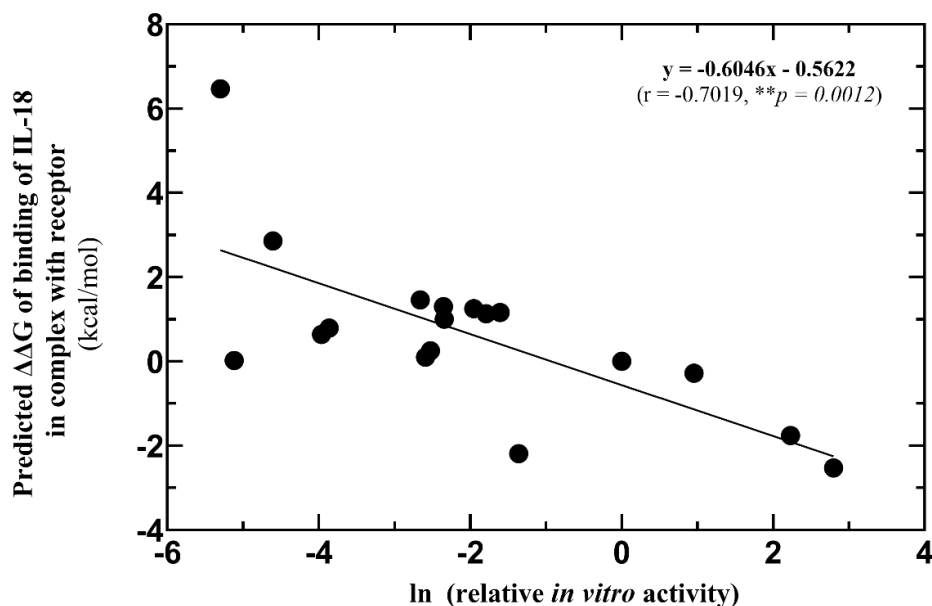


**Figure 12.** Correlation between relative activities of IL-18 and the predicted binding free energies ( $\Delta\Delta G_{\text{binding}}$ ) of IL-18/IL-18R complex obtained from FoldX's interaction energy calculation.  $\Delta\Delta G$  value is expressed in kcal/mol. \*\*Correlation is significant at the 0.01 level ( $p$ -value < 0.01).

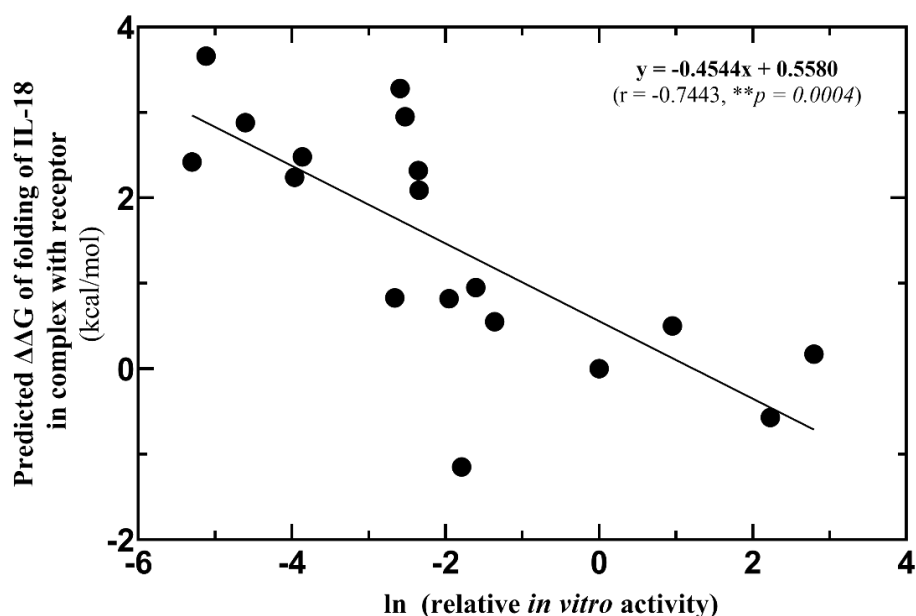


**Figure 13.** Correlation between relative activities of IL-18 and the predicted free energies of folding ( $\Delta\Delta G_{\text{folding of complex}}$ ) of IL-18/IL-18R complex obtained from FoldX's relative free energy calculation.  $\Delta\Delta G$  value is expressed in kcal/mol. \*\*Correlation is significant at the 0.01 level ( $p$ -value < 0.01).

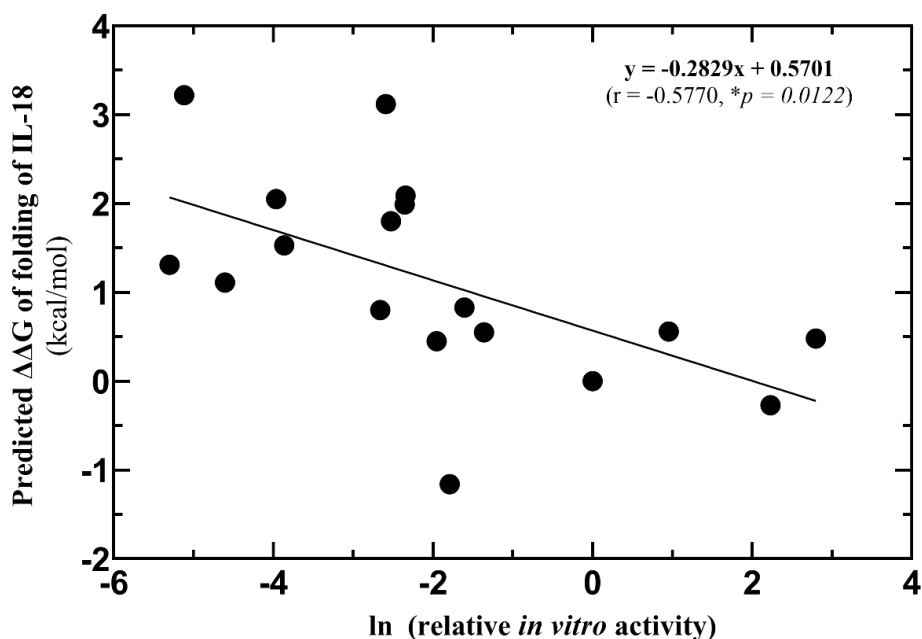


**Figure 14. Correlation between relative activities of IL-18 and the predicted free energies of folding ( $\Delta\Delta G_{\text{folding}}$  of isolated ligand) of IL-18 obtained from FoldX's relative free energy calculation.  $\Delta\Delta G$  value is expressed in kcal/mol. \*Correlation is significant at the 0.05 level ( $p$ -value < 0.05).**

Additionally, we also obtained the equation for activity prediction according to the correlation between experimental activity and three types of predicted free energy ( $\Delta\Delta G$ ) for:

$$\Delta\Delta G_{\text{binding}} : Y = -0.6046x - 0.5622$$

$$\Delta\Delta G_{\text{folding of complex}} : Y = -0.4544x + 0.5580$$

$$\Delta\Delta G_{\text{folding of isolated ligand}} : Y = -0.2829x + 0.5701$$

where Y is estimated the relative free energy ( $\Delta\Delta G$ ) value, X is predicted experimental activity.

According to above mentioned results from the validation process, a significant association between the relative free energy ( $\Delta\Delta G$ ) and *in vitro* activity of IL-18 was observed. A higher  $\Delta\Delta G$  reflected less activity. Therefore, this computational approach was considered as a potential method to obtain quantitatively reliable predicted free energy change ( $\Delta\Delta G$ ) upon mutation, so that could be used for screening the favorable amino acid substitution of IL-18.

### 3.4 *In silico* screening of favorable mutation

To identify potential candidate mutation, we considered the relative free energy change upon mutation in term of  $\Delta\Delta G_{\text{binding}}$ ,  $\Delta\Delta G_{\text{folding of complex}}$ , and  $\Delta\Delta G_{\text{folding of isolated ligand}}$  values as energy-based criterion for selection of favorable mutation. A designed mutation should improve the binding affinity to the receptor as well as preserve the overall conformation stability of IL-18 in both isolated and complex structure. The mutation(s) with favorable energetically contribution or  $\Delta\Delta G < 0$  prones to be potential candidate mutations.

As an activity of IL-18 showed a good correlation with the relative free energy change ( $\Delta\Delta G$ ) upon mutation, we thus decided to rank the promising candidate mutation by using the scoring scheme:

$$\text{Mutation score} = \sum (\Delta\Delta G_{\text{binding}} \times w_1) + (\Delta\Delta G_{\text{folding of complex}} \times w_2) + (\Delta\Delta G_{\text{folding of isolated ligand}} \times w_3).$$

According to the abovementioned equation,  $w_1$ ,  $w_2$  and  $w_3$  are coefficients as -0.702, -0.744, and -0.577 for  $\Delta\Delta G_{\text{binding}}$ ,  $\Delta\Delta G_{\text{folding of complex}}$ , and  $\Delta\Delta G_{\text{folding of isolated ligand}}$ , respectively. The higher score indicated promising design mutation.

#### 3.4.1 Single point mutation study

The single point mutation(s) of amino acid involved in the binding interface was considered as an effective strategy to improve the biological activity and stability of IL-18 (Kim et al., 2001; Underwood et al., 2006; Yamamoto et al., 2004). In our work, the selected unfavorable residues of IL-18 involved in the direct binding to IL-18R were subjected to perform *in silico* saturation mutagenesis by mutating to all other 19 amino acids. Their impacts on IL-18 and IL-18R binding affinities, on IL-18 stability, and on overall stability of IL-18/IL-18R complex were then predicted using our validated computational protocols.

Finally, eleven amino acid points were identified as unfavorable binding residues namely Glu6, Asn41, Arg44, Asp54, Gln56, Asp110, Asn111, Met113, Lys129, Arg131, and Asn155. The changes of free energy ( $\Delta\Delta G$ s) were calculated and shown as the heat maps in Figure 15, Figure 16 and Figure 17, respectively.

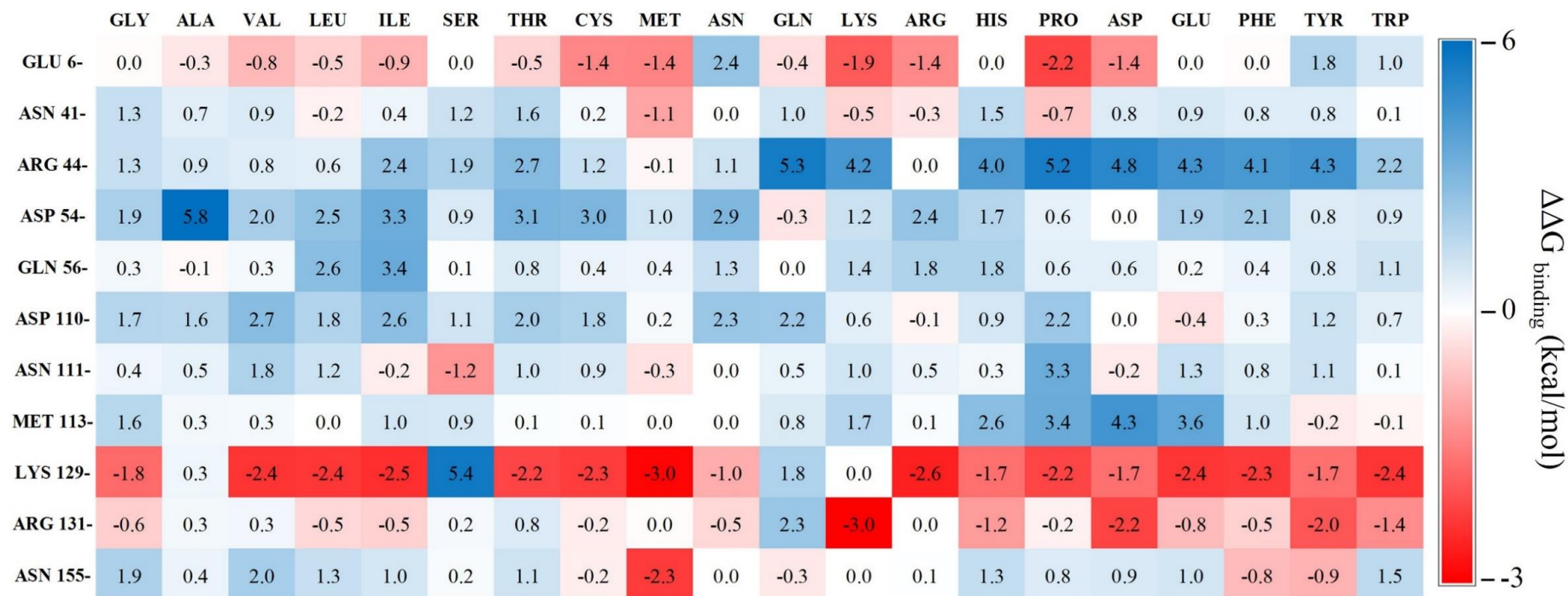


**Figure 15.** Heat map representation of the predicted binding free energy ( $\Delta\Delta G_{\text{binding}}$ ) upon mutation of each 11 unfavorable residues of IL-18. “ $\Delta\Delta G_{\text{binding}}$ ” estimated the change of binding affinity of the wild-type and the mutant variant toward its receptor. Red and blue colored matrices indicate mutations predicted to increase and decrease affinity to receptor compared to wild-type, respectively. All  $\Delta\Delta G$  values are in kcal/mol.

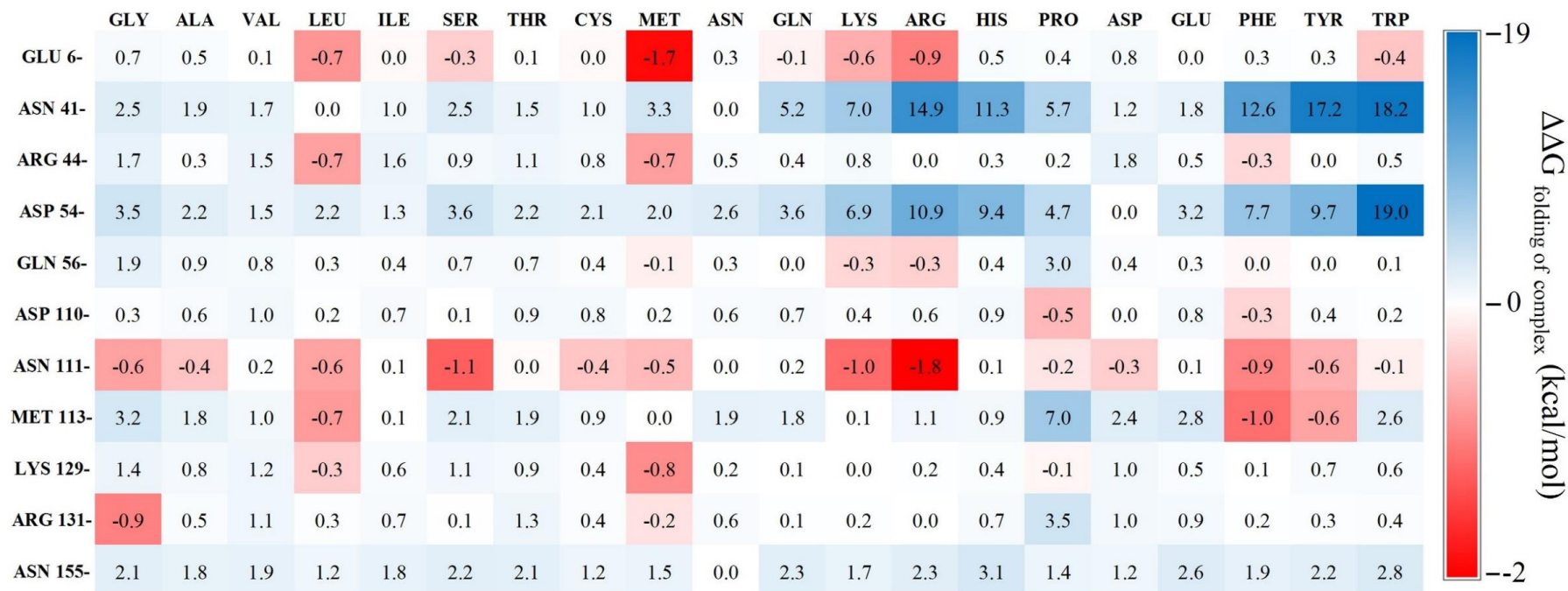


**Figure 16. Heat map representation of the predicted free energy of folding of IL-18/IL-18R complex ( $\Delta\Delta G_{\text{folding of complex}}$ ) upon mutation in each 11 unfavorable residues of IL-18.** “ $\Delta\Delta G_{\text{folding of complex}}$ ” determined the impact of mutations on the stability of the IL-18/IL-18R complex. Red and blue colored matrices indicate stabilization and destabilization of whole complex of mutant toward its receptor with respect to wild-type, respectively. All  $\Delta\Delta G$  values are in kcal/mol.

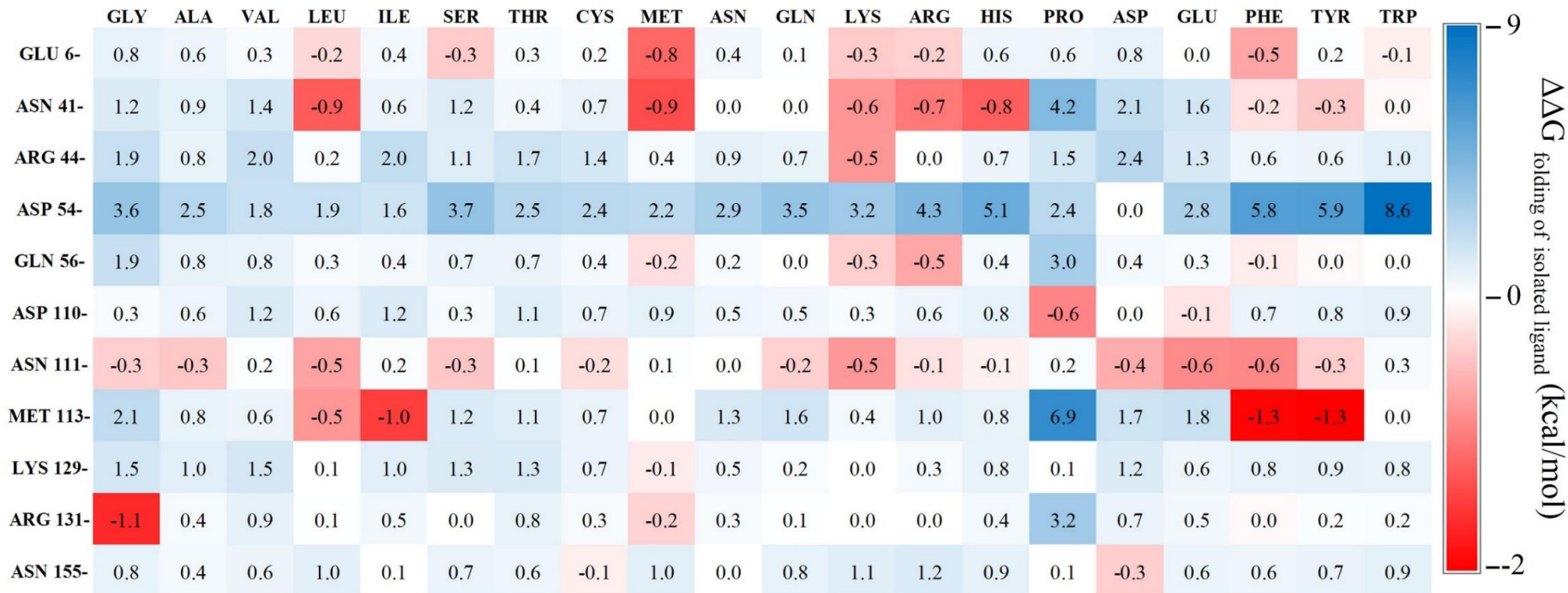


**Figure 17. Heat map representation of the predicted free energies of folding of IL-18 ( $\Delta\Delta G_{\text{folding of isolated ligand}}$ ) upon mutation in each 11 unfavorable residues of IL-18.** “ $\Delta\Delta G_{\text{folding of free IL-18}}$ ” investigated the effect of mutations on the stability of isolated IL-18. Red and blue colored matrices indicate stabilization and destabilization of whole complex of mutant toward its receptor with respect to wild-type, respectively. All  $\Delta\Delta G$  values are in kcal/mol.

A total of 65 (31.1%) of the 209 mutations were predicted to increase affinity to the receptor with favorable binding free energies than the wild-type protein (Figure 15). Considering variant stabilities, 40 (19.1%) mutations were predicted to stabilize the interface of IL-18/IL-18R complex (Figure 16) and 46 (22%) mutations tend to conserve the stability of the isolated IL-18 (Figure 17) due to their favorable free energies compared to the wild-type.

Based on selection criteria, E6M mutant was the best candidate for single point mutation (Table 6). The E6M was consistent with the previous *in vitro* studies that the mutation of E6 to alanine and lysine (E6A and E6K) showed increased activity of IL-18 compared to wild-type (Kim et al., 2001; Kim et al., 2002). These suggested that E6 is a promising target for designing mutation increasing IL-18 activity. However, IL-18 with T63A did not correlate with free energy change upon mutation. This gave us a speculation that our protocol would work well for the case of amino acid(s) at the direct binding IL-18/IL-18R interface because all selected mutations except T63A are the amino acids contributing to binding directly.

**Table 6** *In silico* predicted relative free energy ( $\Delta\Delta G$ ) of the best five variants in single point mutation study ranked by our mutation score. All  $\Delta\Delta G$  values are in kcal/mol.

Mutation	$\Delta\Delta G$ binding	$\Delta\Delta G$ folding of complex	$\Delta\Delta G$ folding of ligand	Score
<i>Control group</i>				
Wild-type <sup>a</sup>	0	0	0	0
E6K <sup>a</sup>	-1.9	-0.6	0.3	1.95
T63A <sup>a</sup>	-0.8	0.8	0.8	-0.44
M60Q <sup>a</sup>	4.6	2.2	0.8	-5.35
M33Q <sup>a</sup>	4.6	2.9	2.7	-7.02
<i>Candidate group</i>				
E6M	-1.4	-1.7	-0.8	2.76

K129M	-3.0	-0.8	-0.1	2.74
R131K	-3.0	0.2	0.0	1.93
N111S	-1.2	-1.1	-0.3	1.87
R131G	-0.6	-0.9	-1.1	1.70

<sup>a</sup>The biological activity of wild-type, E6K (+ve), M33Q (-ve) and M60Q (-ve) mutants were evaluated experimentally by IFN- $\gamma$  induction assay in NK-92MI cells when compared to IL-18 wild-type (Saetang et al., 2016).

### 3.4.2 Double mutation study

In case of IL-18, an increase in biological activity and therapeutic efficacy was observed toward the double mutation in binding residues of IL-18 (Kim et al., 2001; Saetang et al., 2016; Saetang et al., 2020). To predict the synergistic effects, all nine possible mutual combinations of the favorable single mutations were studied. Five single mutation, E6M, K129M, R131K, N111S, and R131G were combined to produce nine double mutant. Table 7 exhibited that all combination of single favorable mutation were predicted to increase in both binding affinity ( $\Delta\Delta G_{\text{binding}}$ ) and stability toward the receptor ( $\Delta\Delta G_{\text{binding}}$ ) and protein itself ( $\Delta\Delta G_{\text{folding of ligand}}$ ) compared to the wild-type. We found that 4 of 5 best double mutants ranked by mutation score are composed of E6M. Interestingly, the best candidate of single point mutation.

**Table 7. *In silico* predicted relative free energy ( $\Delta\Delta G$ ) of the variants in double mutation study ranked by our mutation score. All  $\Delta\Delta G$  values are in kcal/mol.**

Mutation	$\Delta\Delta G_{\text{binding}}$	$\Delta\Delta G_{\text{folding of complex}}$	$\Delta\Delta G_{\text{folding of ligand}}$	Score
<i>Control group</i>				
Wild-type <sup>a</sup>	0	0	0	0
E6K <sup>a</sup>	-1.9	-0.6	0.3	1.95

E6K+T63A <sup>a</sup>	-2.5	0.2	0.5	1.32
M33Q <sup>a</sup>	4.6	2.9	2.7	-7.02
M60Q <sup>a</sup>	4.6	2.2	0.8	-5.35
<b><i>Candidate group</i></b>				
K129M+R131G	-2.0	-2.5	-2.1	4.48
E6M+R131G	-1.9	-2.6	-1.9	4.43
E6M+K129M	-2.3	-2.6	-0.9	4.02
E6M+N111S	-2.0	-2.6	-1.1	3.98
E6M+R131K	-3.4	-1.5	-0.7	3.94
N111S+R131G	-2.2	-1.9	-1.4	3.82
R131K+N111S	-4.0	-0.9	-0.2	3.63
K129M+N111S	-2.6	-2.0	-0.4	3.52
K129M+R131K	-2.4	-0.6	0.0	2.09

---

<sup>a</sup>The biological activity of wild-type, E6K (+ve), E6K+T63A (+ve), M33Q (-ve) and M60Q (-ve) mutants were evaluated experimentally by IFN- $\gamma$  induction assay in NK-92MI cells when compared to IL-18 wild-type (Saetang et al., 2016).

Combinations of E6K+T63A mutations could synergize the augmentation of biological function and clinical application of IL-18 in both *in vitro* and *in vivo* studies (Saetang et al., 2016; Saetang et al., 2020). These results provided additional evidence to support the finding that the presence of synergistic mutational effect of E6 significantly improve the IL-18 activity.

### 3.4.3 Multiple mutation study

Nowadays, directed evolution technique has emerged as a promising strategy for improving the functionality of proteins by increasing mutation rate, resulting the possibility of finding an optimal mutation (Arnold, 1998; Hibbert & Dalby, 2005).

Applying this strategy to our work, we decided to investigate the additive effects by introducing multiple mutation to IL-18. Five single mutations, E6M, K129M, R131K, N111S, and R131G, were combined into seven triple and two quadruple mutation. Predicted values of the changes of free energy ( $\Delta\Delta G$ s) were calculated and summarized in Table 8.

The synergetic energetic effects of the predicted relative free energies ( $\Delta\Delta G$ s) were observed from all variants with multiple mutation. Moreover, the candidate mutants with multiple mutation showed the best mutation score among the three mutation strategies, suggesting that the combination of multiple mutation of IL-18 residue is considered as a potential strategy to improve their biological activity. The previous work reported that combination of S10T+D17N+T63A mutations exhibited 2-fold greater activity compared to wild-type (Underwood et al., 2006). Our computational strategy provided a benefit to identify favorable combinatorial mutations increasing the activity of IL-18.

**Table 8. *In silico* predicted relative free energy ( $\Delta\Delta G$ ) of the variants in multiple mutation study ranked by our mutation score. All  $\Delta\Delta G$  values are in kcal/mol.**

<b>Mutation</b>	<b><math>\Delta\Delta G</math> binding</b>	<b><math>\Delta\Delta G</math> folding of complex</b>	<b><math>\Delta\Delta G</math> folding of ligand</b>	<b>Score</b>
<b><i>Control group</i></b>				
Wild-type <sup>a</sup>	0	0	0	0
E6K <sup>a</sup>	-1.9	-0.6	0.3	1.95
E6K+T63A <sup>a</sup>	-2.5	0.2	0.5	1.32
M33Q <sup>a</sup>	4.6	2.9	2.7	-7.02
M60Q <sup>a</sup>	4.6	2.2	0.8	-5.35
<b><i>Candidate group</i></b>				
E6M+K129M+R131G+N111S	-5.4	-5.6	-3.2	9.78

E6M+N111S+R131G	-4.8	-4.0	-2.2	7.66
E6M+K129M+R131G	-3.7	-4.3	-2.9	7.45
K129M+N111S+R131G	-4.7	-3.8	-2.3	7.45
E6M+K129M+R131K+N111S	-4.8	-3.1	-1.1	6.35
E6M+R131K+N111S	-4.2	-2.3	-1.0	5.27
E6M+K129M+N111S	-2.3	-3.5	-1.2	4.88
E6M+K129M+R131K	-3.5	-2.3	-0.8	4.65
K129M+R131K+N111S	-3.9	-1.7	-0.3	4.13

<sup>a</sup>The biological activity of wild-type, E6K (+ve), E6K+T63A (+ve), M33Q (-ve) and M60Q (-ve) mutants were evaluated experimentally by IFN- $\gamma$  induction assay in NK-92MI cells when compared to IL-18 wild-type (Saetang et al., 2016).

#### 3.4.4 Selection of favorable mutation

As mentioned in previous section, we proposed a computational strategy for identify favorable mutations. Among all possible mutations, the best three candidate mutants, ranked by mutation score, showed the highest binding interaction and structural stabilization compared to other mutations, namely

- E6M+K129M+R131G+N111S
- E6M+N111S+R131G, and
- E6M+K129M+R131G

These variants could be a promising candidates for improving protein activity. Moreover, our findings revealed synergistic mutational effects of E6M mutant when combined with other mutations, suggesting that the modulation of IL-18 activity may have been influenced by Glu6 residue. 3D structure between IL-18 with the selected candidate residues and IL-18R $\alpha$ , as shown in Figure 18.

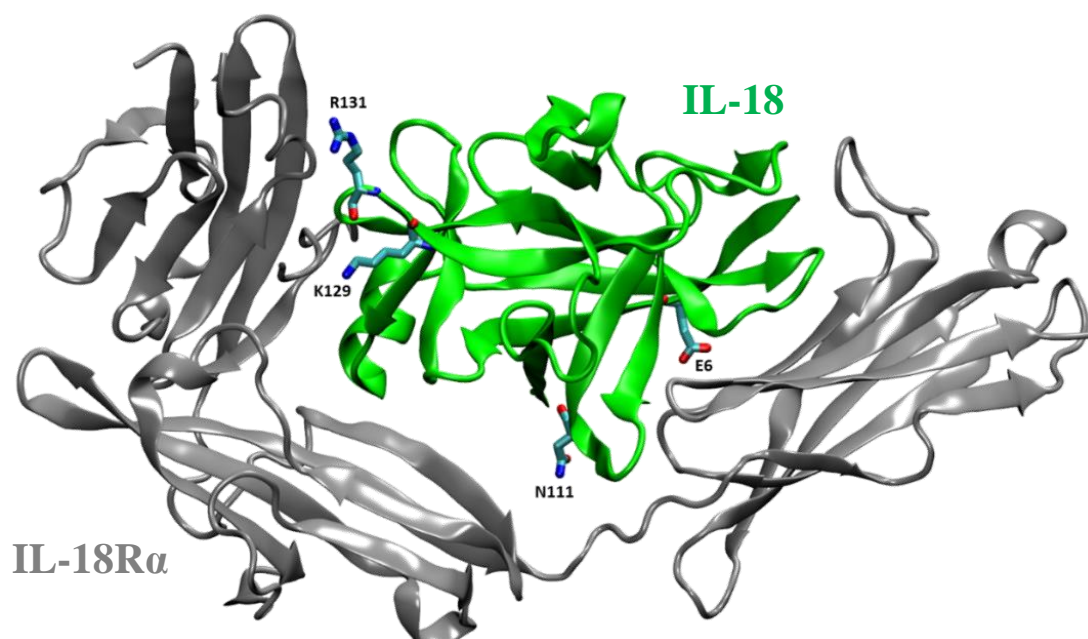


**Figure 18. 3D structure of IL-18 in complex with IL-18R $\alpha$ .** The selected candidate residues (E6, N111, K129 and R131) show in Licorice. The structure of human IL-18 (green) and IL-18R $\alpha$  (grey).

### 3.5 MD simulation analysis of mutations

An atomistic understanding of our selected candidate mutations is essential to rationally guide the computational design of potent and effective IL-18 as a therapeutic candidate. In our work, we used molecular dynamics (MD) simulation to investigate the impacts of these mutations on the structural and functional implications of the protein.

#### 3.5.1 Conformational stability analysis

To study the dynamic stabilities of each simulated model, we performed MD simulation of four candidate mutants (E6M, E6M+N111S+R131G, E6M+K129M+R131G, and E6M+N111S+K129M+R131G) and the model structures with reported *in vitro* activities (wild-type, E6K, and M33Q) for 150 ns at 310K under 1 atm pressure. The Root-Mean-Square Deviation (RMSD) values of all atoms in each model were plotted as depicted in Figure 19.

The RMSD values of all studies systems continuously increased in the first 15 ns and then fluctuated in the range of 1.5 Å during the simulation, suggesting that the systems have reach an equilibrium. Thus, the MD trajectories from last 90 ns were extracted for further analysis. We found that the average RMSD value of wild-type, E6M, E6M+N111S+R131G, E6M+K129M+R131G, E6M+N111S+K129M+R131G, E6K (positive control), and M33Q (negative control) were  $1.78 \pm 0.322$ ,  $1.25 \pm 0.15$ ,  $1.50 \pm 0.23$ ,  $1.34 \pm 0.21$ ,  $1.97 \pm 0.42$ ,  $1.54 \pm 0.29$  and  $1.73 \pm 0.39$  Å, respectively.

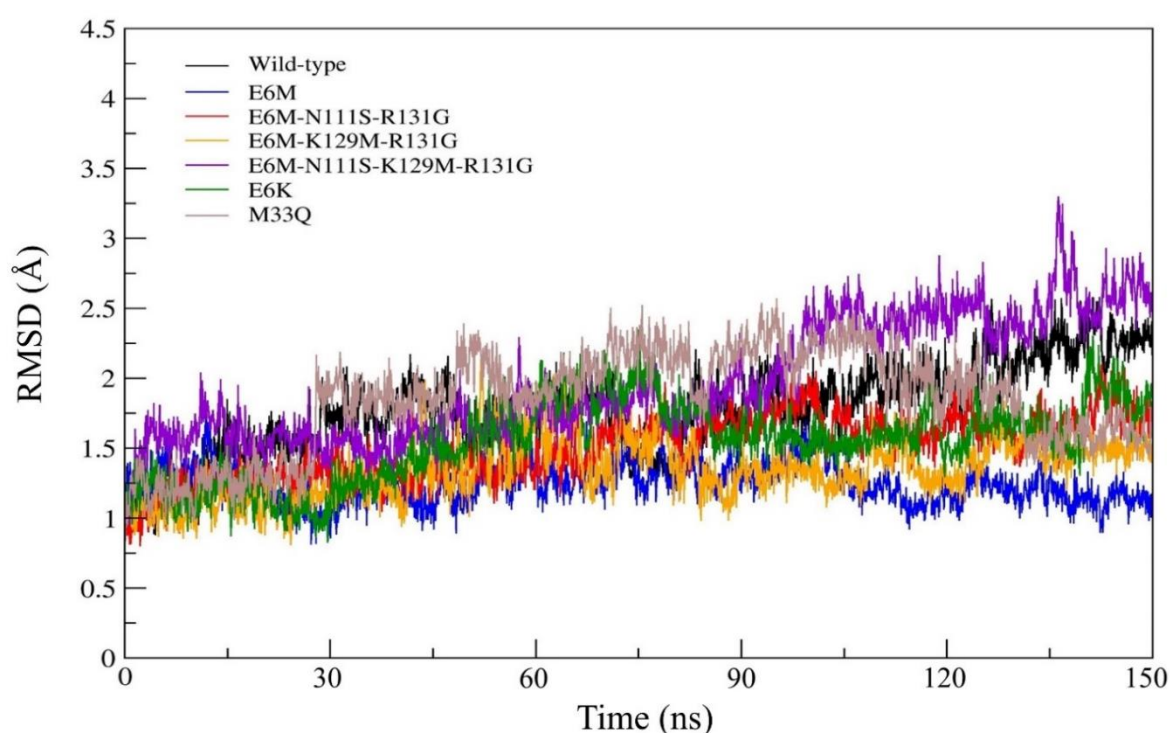


**Figure 19. Root-Mean-Square Deviation (RMSD) plots from the 150 ns MD simulations of all IL-18 structures.** Wild-type (black), E6M (blue), E6M-N111S-R131G (red), E6M-K129M-R131G (yellow), E6M-N111S-K129M-R131G (purple), E6K (green), and M33Q (gray).

### 3.5.2 Structural comparison

Moreover, we also analyzed an average distance of all backbone atoms in each amino acid from an origin point. The distance pattern was compared among the wild-type and mutant structures. A difference in average distance of corresponding amino acids indicated the structural alternation at the atomistic level. The average distance of the geometric center of backbone atoms (N, C, C $\alpha$ , and O atoms) to an origin point

(0,0,0) in each simulated structures in angstrom ( $\text{\AA}$ ) unit were calculated from the last 1000 MD trajectories. The conformational comparison by distance pattern exhibited that there is no significant difference in the average distance of backbones atoms in each amino acids between the wild-type and mutant structures of IL-18 (Figure 20).

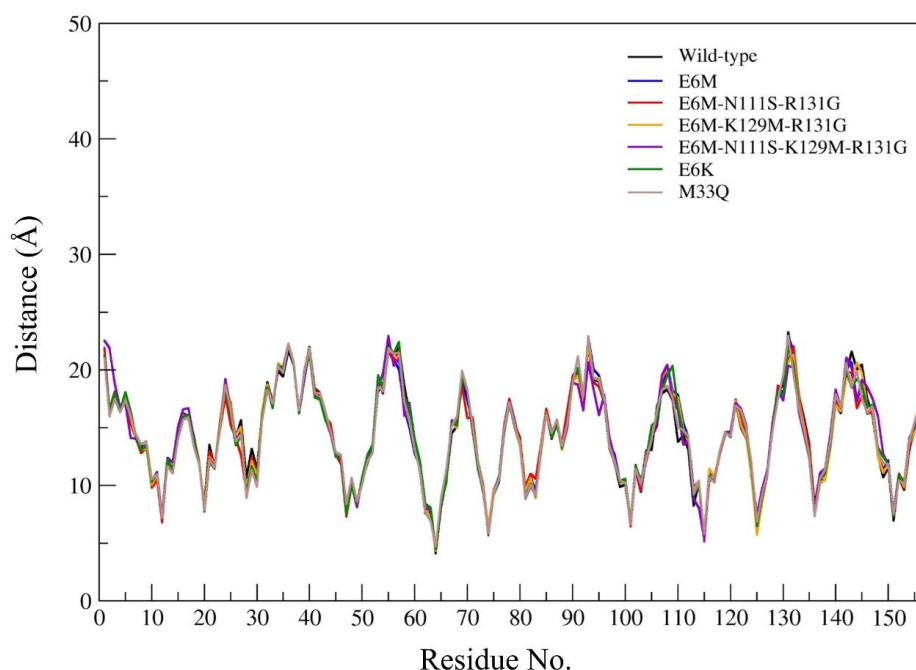


**Figure 20. Average distance pattern in Angstrom units of all atoms in each IL-18 structures during MD simulation.** Wild-type (black), E6M (blue), E6M-N111S-R131G (red), E6M-K129M-R131G (yellow), E6M-N111S-K129M-R131G (purple), E6K (green), and M33Q (gray).

Taken together, the superimposition of the protein structures (Figure 21) also confirmed the structural conservation of our mutated IL-18 with respect to the native protein. The results demonstrated that the protein structure of IL-18 wild-type and all mutants could be aligned through the backbone atoms with the generally acceptable range of the RMSD below  $3 \text{ \AA}$ . In agreement with previous work, molecular dynamics and functional studies of IL-18 reported the structural perseverance was primarily responsible for triggering the biological activity of the protein (Saetang et al., 2016). Therefore, these results suggested that our candidate mutations had no effect on the overall conformation of IL-18.

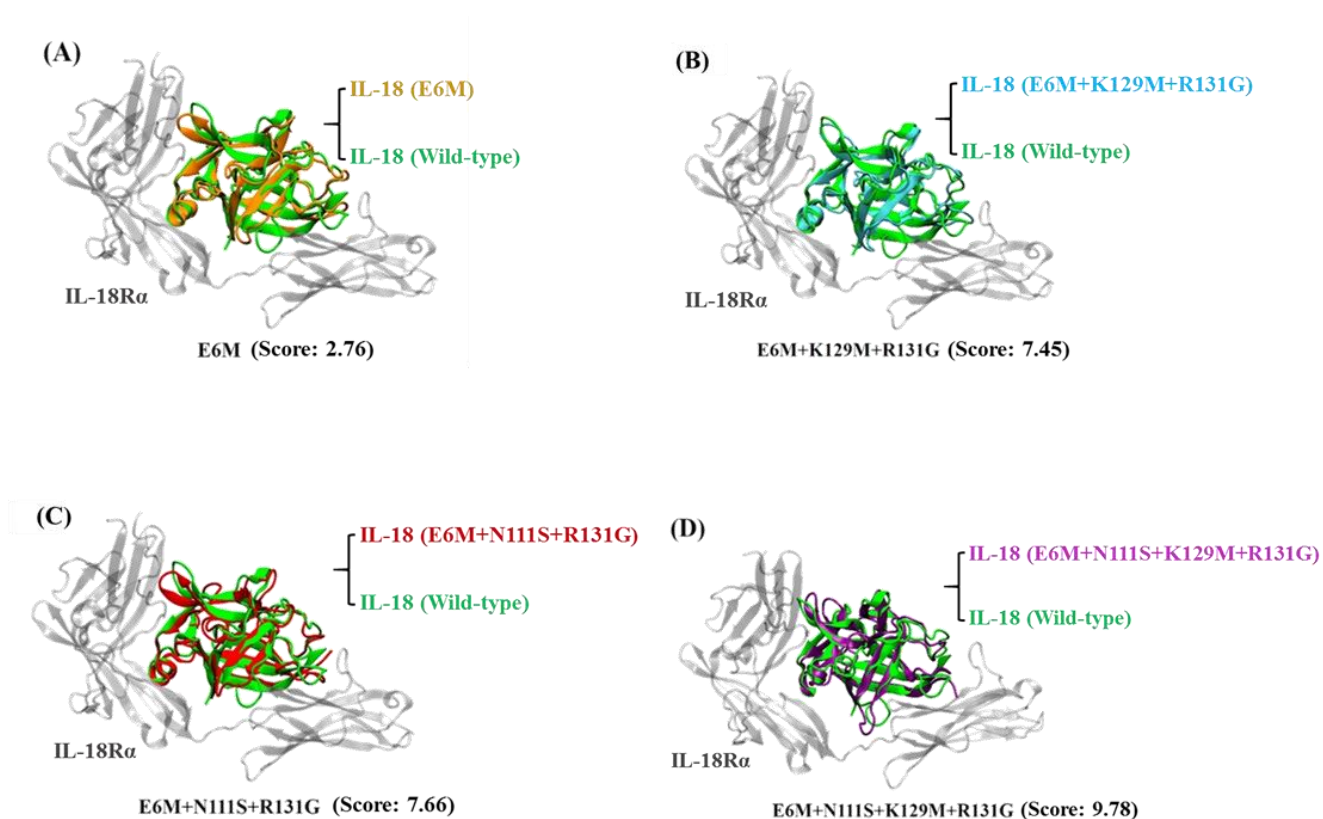


**Figure 21.** The superimposition of the average structure from last 90 ns of simulation of IL-18 wild-type (green) and its mutants (colors) in complex with IL-18R $\alpha$  (gray). Wild-type (green), E6M (orange), E6M-N111S-R131G (red), E6M-K129M-R131G (cyan) and E6M-N111S-K129M-R131G (purple).

### 3.5.3 Hydrogen bond analysis

Since the biological function of proteins depends on their stable configuration, hydrogen bonding interaction play a fundamental role in stabilizing the three-dimensional structure of protein. To gain insight into the hydrogen bond details from the IL-18 wild-type and mutants, the number of intra-molecular hydrogen bonds in each protein structures were analyzed using the final 90 ns MD trajectories according to the subsequent criteria (1) the distance between proton donor (D) and acceptor (A) atoms was less than 3.5 Å, and (2) HD-H $\cdots$ HA angle of at least 150°, as presented in Figure 22.

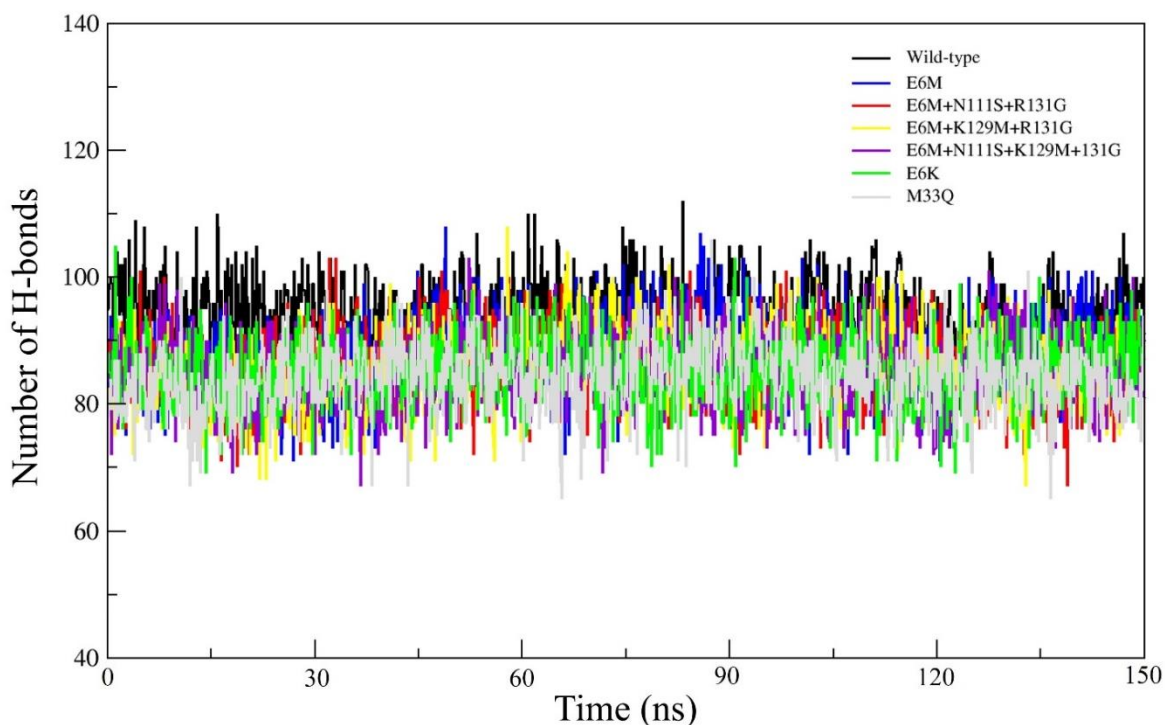


**Figure 22. Hydrogen bond profiles of all IL-18 structures during MD simulation.** Wild-type (black), E6M (blue), E6M-N111S-R131G (red), E6M-K129M-R131G (yellow), E6M-N111S-K129M-R131G (purple), E6K (green), and M33Q (gray).

We found that the average intra-molecular hydrogen bond of IL-18 wild-type, E6M, E6M+N111S+R131G, E6M+K129M+R131G, E6M+N111S+K129M+R131G, E6K, and M33Q were 94, 88, 86, 86, 85, 85, and 84 H-bonds, respectively. These results showed a minimum difference in the hydrogen bond formation between the candidate mutant structures and the protein structures with experimentally reported activities (wild-type, E6K, and M33Q mutants). These suggested that our candidate mutants were able to maintain their overall conformation through the stabilization from the intra-molecular hydrogen bond. However, the number of intra-molecular hydrogen bonds were observed to slightly decrease in all mutated IL-18 structures compared to the wild-type protein, suggesting that the alteration of amino acid might trigger a small conformational change in the individual region of IL-18.

### 3.5.4 Structural flexibility analysis

Apart from the conformational stability, structural flexibility was observed in order to examine the effects associated with the mutations on the dynamic behavior of IL-18. The root-mean-square fluctuations (RMSF) of all C $\alpha$  atom in each simulated structures were analyzed to identify the most flexible regions in protein structure. The higher RMSF value indicates more flexible region whereas the lower RMSF value means less flexible region. In this study, the RMSF values of each simulated structures were calculated using the final 90 ns MD trajectories and were then plotted against the residue order of protein, as shown in Figure 23.

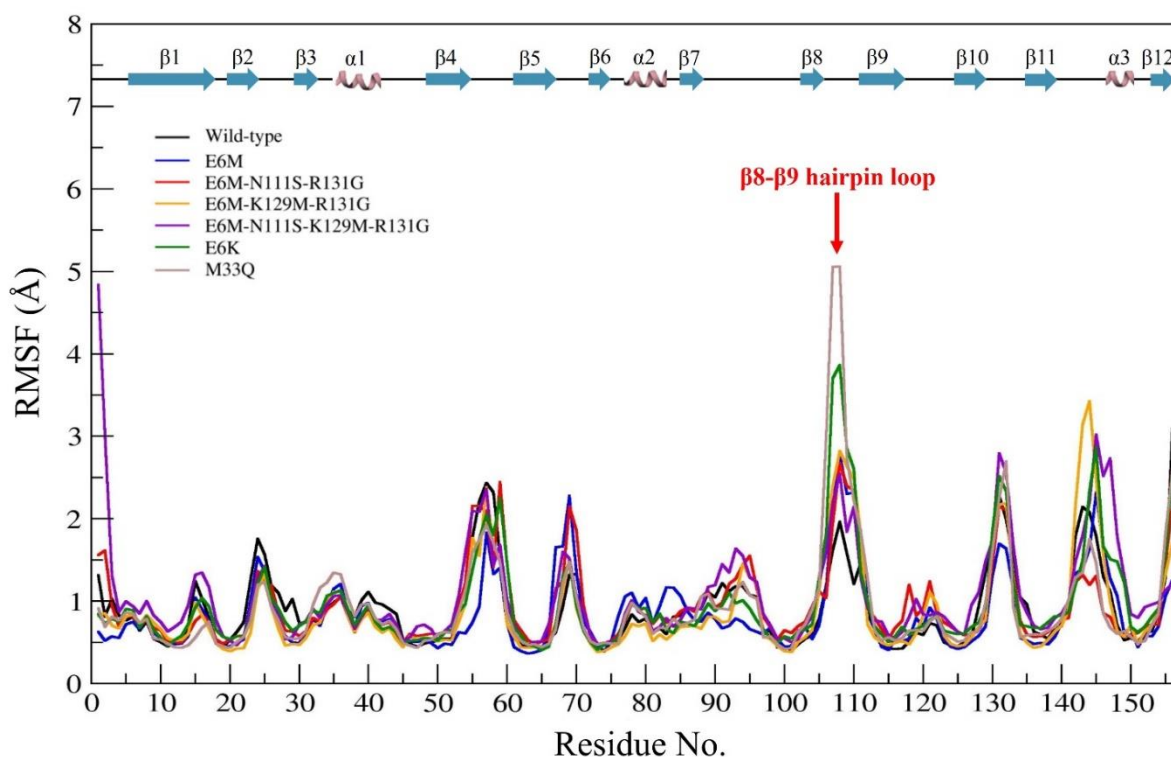


**Figure 23. Root-Mean-Square fluctuation (RMSF) plots of all IL-18 structures during MD simulation.** Wild-type (black), E6M (blue), E6M-N111S-R131G (red), E6M-K129M-R131G (yellow), E6M-N111S-K129M-R131G (purple), E6K (green), and M33Q (gray).

Comparison of the wild-type structure and the mutated structures of IL-18 exhibited that the RMSF profile of the mutants IL-18 showed a similar pattern to that of the wild-type in most of the overall structure. However, we observed that the

fluctuation in amino acid residues, from V106 to K112, of all mutated IL-18 structure were higher than the native protein structure, especially in M33Q (negative control) and E6K (positive control) mutant. This results revealed the induction of the flexibility at V106 to K112 residue could cause the alteration of the  $\beta$ 8- $\beta$ 9 hairpin loop direction of the candidate mutants to provide closer contact with the IL-18R $\beta$  leading to the better binding affinity to its receptor (Figure 24). Moreover, these residues also involved in the binding site III of IL-18 that required for the activation of the IL-18 function through the formation of ternary complex with the receptors (Kato et al., 2003; Tsutsumi et al., 2014). Therefore, our simulations suggested that the increased dynamics of  $\beta$ 8- $\beta$ 9 hairpin loop could have contributed to the biological activity of IL-18 variants.

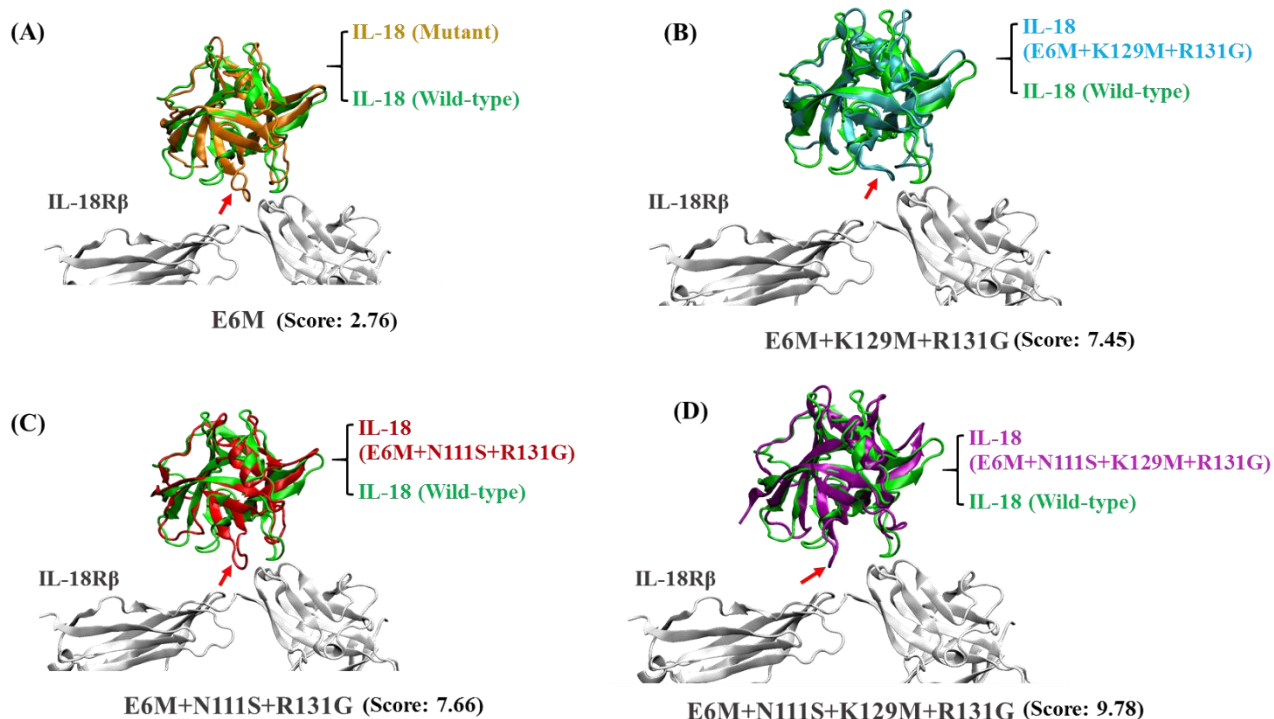


**Figure 24.** The superimposition of the average structure from last 90 ns of simulation of IL-18 wild-type (green) and its mutants (colors) in complex with IL-18R $\beta$  (gray). Wild-type (green), E6M (orange), E6M-N111S-R131G (red), E6M-K129M-R131G (cyan) and E6M-N111S-K129M-R131G (purple). Red arrow indicated the amino acid residues involved in  $\beta$ 8- $\beta$ 9 loop region of IL-18 mutants bind closer to the receptor (IL-18R $\beta$ ) compared to the wild-type.

### 3.5.4 Binding interaction analysis

Analysis of binding interaction between the IL-18 mutants and IL-18R(s) was performed to elucidate the functional significance of the four mutation candidates in context of the receptor binding. The interaction of each simulated structures toward its receptors were analyzed and visualized using VMD software. The interaction profiles of the key residues at the interface between the IL-18R(s) and the candidate mutants, E6M, E6M+K129M+R131G, E6M+N111S+R131G were summarized in Table 9, 10, 11 and 12, respectively.

**Table 9. Binding interactions between the E6M mutant/IL-18R interfaces at binding site I, II and III.**

Binding site	IL-18 residue	IL-18R residue	Interaction
<b>Site I</b>	D17	K128	Electrostatic interaction
	D32	R25	Electrostatic interaction
	D40	H27	Electrostatic interaction
	D132	K39	Electrostatic interaction
<b>Site II</b>	K53	E263	Electrostatic interaction
<b>Site III</b>	D110	K313	Electrostatic interaction
	K112	E210	Electrostatic interaction
	K112	Y212	Cation- $\pi$ interaction
	R147	E210	Electrostatic interaction

**Table 10. Binding interactions between the E6M+K129M+R131G mutant/IL-18R interfaces at binding site I, II and III.**

<b>Binding site</b>	<b>IL-18 residue</b>	<b>IL-18R residue</b>	<b>Interaction</b>
	D17	K128	Electrostatic interaction
	D32	R25	Electrostatic interaction
<b>Site I</b>	D40	H27	Electrostatic interaction
	D40	R123	Electrostatic interaction
	D132	K39	Electrostatic interaction
<b>Site II</b>	K53	E263	Electrostatic interaction
	H109	E210	Electrostatic interaction
	D110	K313	Electrostatic interaction
<b>Site III</b>	K112	E210	Electrostatic interaction
	K112	Y212	Cation- $\pi$ interaction
	R147	E210	Electrostatic interaction

**Table 11. Binding interactions between the E6M+N111S+R131G mutant/IL-18R interfaces at binding site I, II and III.**

<b>Binding site</b>	<b>IL-18 residue</b>	<b>IL-18R residue</b>	<b>Interaction</b>
<b>Site I</b>	D17	K128	Electrostatic interaction
	D32	R25	Electrostatic interaction
	D40	H27	Electrostatic interaction
	D132	K39	Electrostatic interaction
<b>Site II</b>	K53	E263	Electrostatic interaction
<b>Site III</b>	H109	E210	Electrostatic interaction
	H109	Y212	$\pi$ - $\pi$ stacking / cation- $\pi$ interaction
	D110	K313	Electrostatic interaction
	K112	E210	Electrostatic interaction
	K112	Y212	Cation- $\pi$ interaction
	R147	E210	Electrostatic interaction

**Table 12. Binding interactions between the E6M+N111S+K129M+R131G mutant/IL-18R interfaces at binding site I, II and III.**

<b>Binding site</b>	<b>IL-18 residue</b>	<b>IL-18R residue</b>	<b>Interaction</b>
	D17	K128	Electrostatic interaction
	D17	F202	Anion- $\pi$ interaction
	D32	R25	Electrostatic interaction
<b>Site I</b>	D37	R25	Electrostatic interaction
	D40	H27	Electrostatic interaction
	D40	R123	Electrostatic interaction
	D132	K39	Electrostatic interaction
<b>Site II</b>	K53	Y248	Cation- $\pi$ interaction
	H109	E210	Electrostatic interaction
	D110	E210	Electrostatic interaction
<b>Site III</b>	K112	E210	Electrostatic interaction
	K112	Y212	Cation- $\pi$ interaction
	D146	Y214	Anion- $\pi$ interaction

The results exhibited the similarity between the binding interactions of four candidate mutants to the receptors. E6M mutant revealed 8 possible binding residues involved in the receptor binding site I, II and III, including D17, D32, D40, K53, D110, K112, D132, and R147. While E6M+K129M+R131G and E6M+N111S+R131G mutants exhibited 9 binding residues, such as D17, D32, D40, K53, H109, D110, K112, D132, and R147. Interestingly, the best candidate mutant, E6M+N111S+K129M+R131G, showed the most favorable binding interaction to its receptors via 10 binding residues, including D17, D32, D37, D40, K53, H109, D110, K112, D132, and R147.

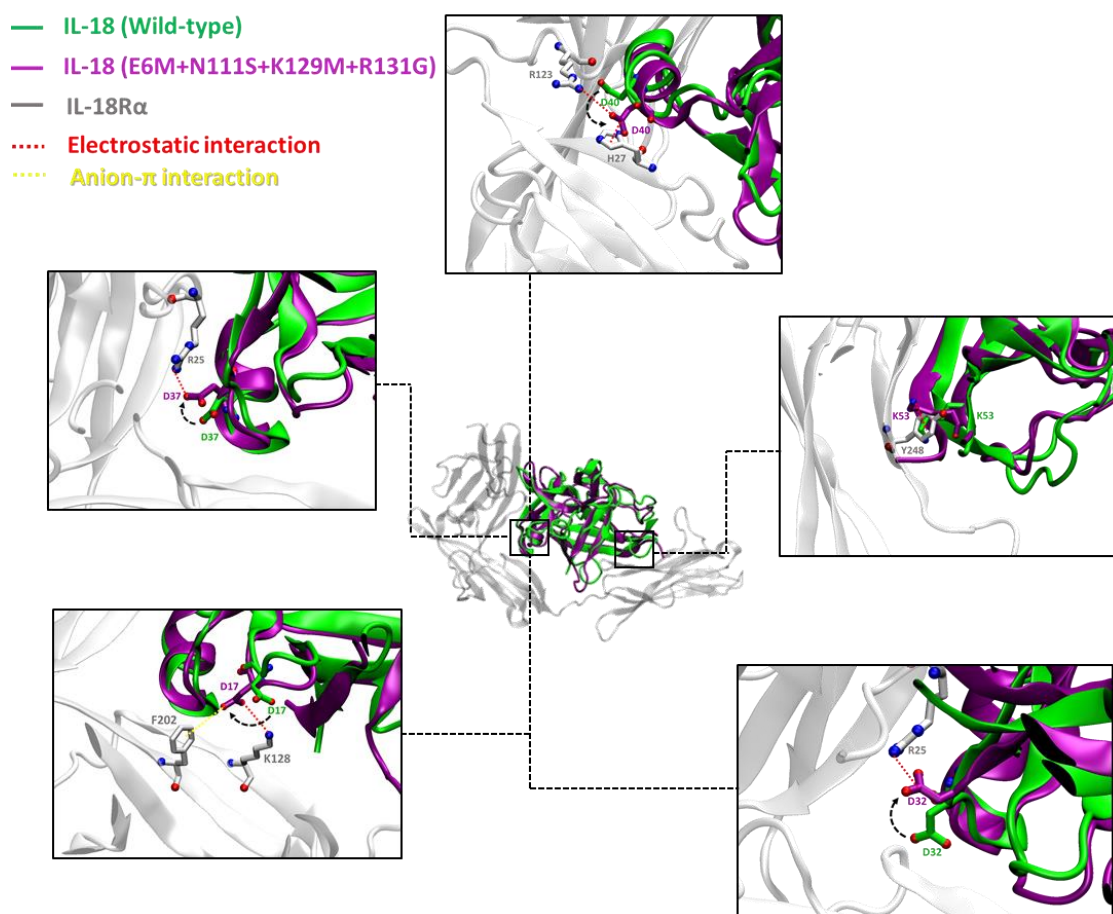


**Figure 25.** Binding interaction of IL-18 with E6M+N111S+K129M+R131G mutation (purple) and IL-18R $\alpha$  (gray) at the receptor binding site I and II compared to wild-type (green). The electrostatic interactions are shown as red dashed lines, and the anion- $\pi$  interaction is shown in yellow dashed line.

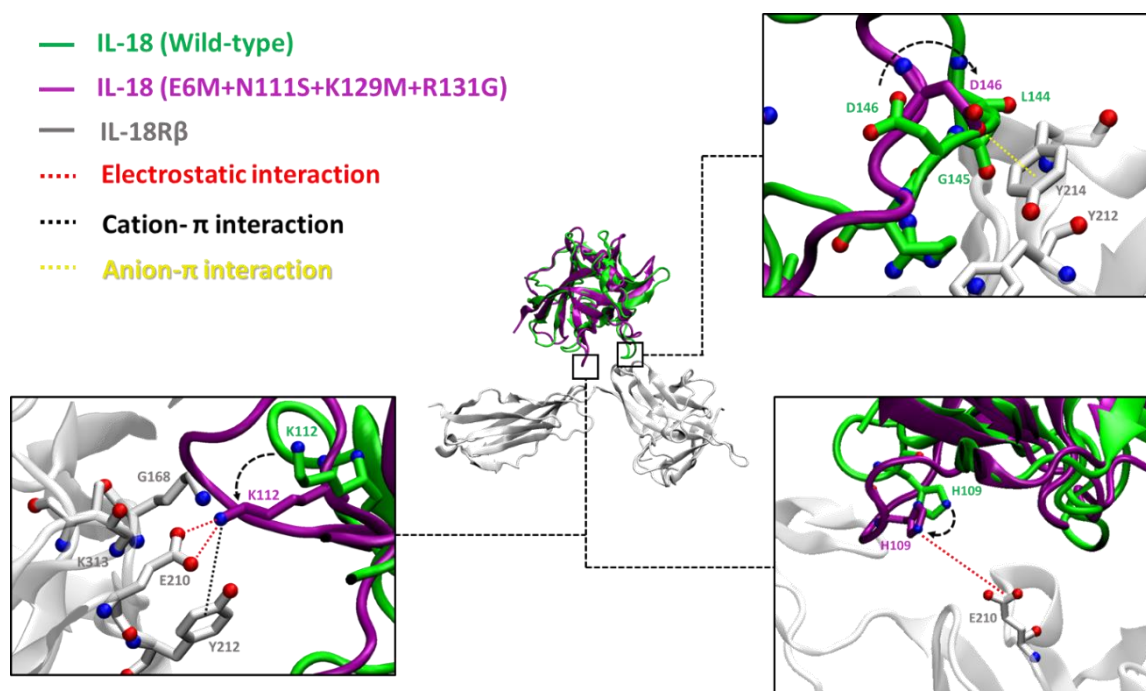


**Figure 26. Binding interaction of IL-18 with E6M+N111S+K129M+R131G mutation (purple) and IL-18R $\beta$  (gray) at the receptor binding site III compared to wild-type (green).** The electrostatic interactions are shown as red dashed lines, the cation- $\pi$  interaction is shown black dashed line, and the anion- $\pi$  interaction is shown in yellow dashed line.

Atomistic insights revealed that the key residues of E6M+N111S+K129M+R131G mutant at the interface of the IL-18/IL-18R complex make closer contact to IL-18R $\alpha$  (site I and II) and IL-18R $\beta$  (site III), as shown in Figure 25 and 26, respectively. Therefore, the results were consistent with the predicted free energy contribution showing that our candidate mutants could improve the IL-18 receptor binding and the main contributions to the binding interactions were from electrostatic interactions.

## CHAPTER 4

### CONCLUSION

The idea of structure-guided protein design is to exploit the information from the detailed analysis of the structure, function, and protein-protein interactions at an atomistic level to design a new promising protein. In this study, the integration of computational structure-based energy calculation and molecular dynamic simulations were used to screen and identify candidate mutations increasing the activity of IL-18 based on hypothesis that the favorable energetic contribution and structural conservation is needed for the receptor recognition of IL-18. Thus, the amino acid substitution of IL-18 that had a favorable energetic contributions and preserved the conformation of protein than the native protein may serve as a promising candidate for cytokine-based cancer drugs.

To validate the method, the eighteen *in vitro* functional studies reported structures were subjected to the same computational analyses, where the predicted relative free energy ( $\Delta\Delta G$ ) values were found to be in good agreement with the experimental biological activities of IL-18. According to the ranked predicted  $\Delta\Delta G$  values from the 209 possible single point mutations of the selected unfavorable binding residues, the E6M mutation was predicted to have to the most energetically favorable contribution towards the stabilizing and binding to the receptor than other mutations. The combination of E6M with other favorable mutations, including E6M+N111S+R131G, E6M+K129M+R131G and E6M+N111S+K129M+R131G exhibited synergistic effect, which could improve their energetic contributions indicated alternative strategy for designing the IL-18 with enhanced activity.

In order to elucidate the conformation stability and dynamic behavior of our designed variants in biological condition, the four potential candidate mutations were then studied by all-atom MD simulation for 150 ns at biological pH condition. The results indicated that both point mutation and multiple mutations on the IL-18 structure had no impact on the overall conformation and foldability of the protein. The MD simulations also observed the increased in the structural flexibility of the  $\beta 8$ - $\beta 9$

hairpin loop of the IL-18 mutants. Due to its involvement of  $\beta 8$ - $\beta 9$  hairpin loop in IL-18 receptor binding, the structural change caused by mutations may alter the biological function of the protein. Moreover, our designed IL-18 with E6M, E6M+N111S+R131G, E6M+K129M+R131G and E6M+N111S+K129M+R131G mutation could promote the better binding affinity to its receptor via increasing electrostatic interactions from the binding residues involved in binding site I, II and III, leading to improving biological activity of IL-18. These results suggested that our computational designed IL-18 with interfacial amino acid modification could be the potential candidates of cytokine-mediated immunotherapy for cancer treatment. Therefore, our present findings provided information for designing promising cytokine. However, our design strategy can be applied to only an amino acid which bound directly to IL-18R. In addition, the effects associated with the mutation on the IL-18 activity still need to be validated experimentally.

## REFERENCES

1. Akira S. The role of IL-18 in innate immunity. *Current opinion in immunology*. 2000;12(1):59-63.
2. Arnold FH. Design by directed evolution. *Accounts of chemical research*. 1998;31(3):125-131.
3. Berendsen HJ, Postma JV, van Gunsteren WF, DiNola A, Haak, JR. Molecular dynamics with coupling to an external bath. *The Journal of Chemical Physics*. 1984;81(8):3684-90.
4. Case DA, Berryman J, Betz RM, Cerutti DS, Cheatham Iii TE, Darden TA, Duke RE, Giese TJ, Gohlke H, Goetz AW, Homeyer N. AMBER 2015.
5. Childers MC, Daggett V. Insights from molecular dynamics simulations for computational protein design. *Molecular systems design & engineering*. 2017;2(1):9-33.
6. Coughlin CM, Salhany KE, Wysocka M, Aruga E, Kurzawa H, Chang AE, Hunter CA, Fox JC, Trinchieri G, Lee WM. Interleukin-12 and interleukin-18 synergistically induce murine tumor regression which involves inhibition of angiogenesis. *The Journal of clinical investigation*. 1998 Mar 15;101(6):1441-52.
7. Darden T, York D, Pedersen L. Particle mesh Ewald: An  $N \cdot \log(N)$  method for Ewald sums in large systems. *The Journal of chemical physics*. 1993 Jun 15;98(12):10089-92.
8. Delgado J, Radusky LG, Cianferoni D, Serrano L. FoldX 5.0: working with RNA, small molecules and a new graphical interface. *Bioinformatics*. 2019 Oct 15;35(20):4168-9.
9. Dinarello CA. Interleukin-18. *Methods*. 1999 Sep 1;19(1):121-32.
10. Dinarello C, Novick D, Kim S, Kaplanski G. Interleukin-18 and IL-18 binding protein. *Frontiers in immunology*. 2013 Oct 8;4:289.
11. Farkona S, Diamandis EP, Blasutig IM. Cancer immunotherapy: the beginning of the end of cancer?. *BMC medicine*. 2016 Dec;14(1):1-8.

12. Fleishman SJ, Whitehead TA, Ekiert DC, Dreyfus C, Corn JE, Strauch EM, Wilson IA, Baker D. Computational design of proteins targeting the conserved stem region of influenza hemagglutinin. *Science*. 2011 May 13;332(6031):816-21.
13. Hao J, Serohijos AW, Newton G, Tassone G, Wang Z, Sgroi DC, Dokholyan NV, Basilion JP. Identification and rational redesign of peptide ligands to CRIP1, a novel biomarker for cancers. *PLoS Comput Biol*. 2008 Aug 1;4(8):e1000138.
14. Hashimoto W, Osaki T, Okamura H, Robbins PD, Kurimoto M, Nagata S, Lotze MT, Tahara H. Differential antitumor effects of administration of recombinant IL-18 or recombinant IL-12 are mediated primarily by Fas-Fas ligand-and perforin-induced tumor apoptosis, respectively. *The Journal of Immunology*. 1999 Jul 15;163(2):583-9.
15. Hibbert EG, Dalby PA. Directed evolution strategies for improved enzymatic performance. *Microbial Cell Factories*. 2005 Dec;4(1):1-6.
16. Cann SH, Van Netten JP, Van Netten C. Dr William Coley and tumour regression: a place in history or in the future. *Postgraduate medical journal*. 2003 Dec 1;79(938):672-80.
17. Huang PS, Boyken SE, Baker D. The coming of age of de novo protein design. *Nature*. 2016 Sep;537(7620):320-7.
18. Humphrey W, Dalke A, Schulten K. VMD: visual molecular dynamics. *Journal of molecular graphics*. 1996 Feb 1;14(1):33-8.
19. Hwang I, Park S. Computational design of protein therapeutics. *Drug Discovery Today: Technologies*. 2008 Sep 1;5(2-3):e43-8.
20. Istivan TS, Pirogova E, Gan E, Almansour NM, Coloe PJ, Cosic I. Biological effects of a de novo designed myxoma virus peptide analogue: evaluation of cytotoxicity on tumor cells. *PLoS One*. 2011 Sep 19;6(9):e24809.
21. Jorgensen WL, Chandrasekhar J, Madura JD, Impey RW, Klein ML. Comparison of simple potential functions for simulating liquid water. *The Journal of chemical physics*. 1983 Jul 15;79(2):926-35.

22. Kato Z, Jee J, Shikano H, Mishima M, Ohki I, Ohnishi H, Li A, Hashimoto K, Matsukuma E, Omoya K, Yamamoto Y. The structure and binding mode of interleukin-18. *Nature Structural & Molecular Biology*. 2003 Nov;10(11):966-71.
23. Kim R. Cancer immunoediting: from immune surveillance to immune escape. *Cancer Immunotherapy*. 2007 Jan 1:9-27.
24. Kim SH, Azam T, Yoon DY, Reznikov LL, Novick D, Rubinstein M, Dinarello CA. Site-specific mutations in the mature form of human IL-18 with enhanced biological activity and decreased neutralization by IL-18 binding protein. *Proceedings of the National Academy of Sciences*. 2001 Mar 13;98(6):3304-9.
25. Kim SH, Azam T, Novick D, Yoon DY, Reznikov LL, Bufler P, Rubinstein M, Dinarello CA. Identification of amino acid residues critical for biological activity in human interleukin-18. *Journal of Biological Chemistry*. 2002 Mar 29;277(13):10998-1003.
26. Koury J, Lucero M, Cato C, Chang L, Geiger J, Henry D, Hernandez J, Hung F, Kaur P, Teskey G, Tran A. Immunotherapies: exploiting the immune system for cancer treatment. *Journal of immunology research*. 2018 Mar 14;2018.
27. Kozakov D, Hall DR, Xia B, Porter KA, Padhorny D, Yueh C, Beglov D, Vajda S. The ClusPro web server for protein–protein docking. *Nature protocols*. 2017 Feb;12(2):255.
28. Kunert A, Chmielewski M, Wijers R, Berrevoets C, Abken H, Debets R. Intra-tumoral production of IL18, but not IL12, by TCR-engineered T cells is non-toxic and counteracts immune evasion of solid tumors. *Oncoimmunology*. 2018 Jan 2;7(1):e1378842.
29. Lee S, Margolin K. Cytokines in cancer immunotherapy. *Cancers*. 2011 Dec;3(4):3856-93.
30. Ma Z, Li W, Yoshiya S, Xu Y, Hata M, El-Darawish Y, Markova T, Yamanishi K, Yamanishi H, Tahara H, Tanaka Y. Augmentation of immune checkpoint cancer immunotherapy with IL18. *Clinical Cancer Research*. 2016 Jun 15;22(12):2969-80.

31. Marcos E, Silva DA. Essentials of de novo protein design: Methods and applications. *Wiley Interdisciplinary Reviews: Computational Molecular Science*. 2018 Nov;8(6):e1374.
32. Martinović KM, Babović N, Džodić R, Jurišić V, Matković S, Konjević G. Favorable in vitro effects of combined IL-12 and IL-18 treatment on NK cell cytotoxicity and CD25 receptor expression in metastatic melanoma patients. *Journal of translational medicine*. 2015 Dec;13(1):1-4.
33. Mittal D, Gubin MM, Schreiber RD, Smyth MJ. New insights into cancer immunoediting and its three component phases—elimination, equilibrium and escape. *Current opinion in immunology*. 2014 Apr 1;27:16-25.
34. Morales A, Eidinger D, Bruce AW. Intracavitary Bacillus Calmette-Guerin in the treatment of superficial bladder tumors. *The Journal of urology*. 2002 Feb 1;167(2):891-4.
35. Murphy JF. *Frontiers in Cancer Immunotherapy*. In: Rezaei N, editor. *Cancer Immunology: Bench to Bedside Immunotherapy of Cancers*. 1st ed. Berlin: Springer-Verlag Berlin Heidelberg, 2015, 1-17.
36. Nakanishi K. Unique action of interleukin-18 on T cells and other immune cells. *Frontiers in immunology*. 2018 Apr 20;9:763.
37. Nishio S, Yamada N, Ohyama H, Yamanegi K, Nakasho K, Hata M, Nakamura Y, Fukunaga S, Futani H, Yoshiya S, Ueda H. Enhanced suppression of pulmonary metastasis of malignant melanoma cells by combined administration of  $\alpha$ -galactosylceramide and interleukin-18. *Cancer science*. 2008 Jan;99(1):113-20.
38. Nutho B, Mahalapbutr P, Hengphasatporn K, Pattarangoon NC, Simanon N, Shigeta Y, Hannongbua S, Rungrotmongkol T. Why are lopinavir and ritonavir effective against the newly emerged coronavirus 2019? Atomistic insights into the inhibitory mechanisms. *Biochemistry*. 2020 Apr 15;59(18):1769-79.
39. Oiseth SJ, Aziz MS. Cancer immunotherapy: a brief review of the history, possibilities, and challenges ahead. *Journal of cancer metastasis and treatment*. 2017 Oct 31;3:250-61.

40. Osaki T, Hashimoto W, Gambotto A, Okamura H, Robbins PD, Kurimoto M, Lotze MT, Tahara H. Potent antitumor effects mediated by local expression of the mature form of the interferon- $\gamma$  inducing factor, interleukin-18 (IL-18). *Gene therapy*. 1999 May;6(5):808-15.
41. Robertson MJ, Mier JW, Logan T, Atkins M, Koon H, Koch KM, Kathman S, Pandite LN, Oei C, Kirby LC, Jewell RC. Clinical and biological effects of recombinant human interleukin-18 administered by intravenous infusion to patients with advanced cancer. *Clinical Cancer Research*. 2006 Jul 15;12(14):4265-73.
42. Romero-Durana M, Jiménez-García B, Fernández-Recio J. pyDockEneRes: per-residue decomposition of protein–protein docking energy. *Bioinformatics*. 2020 Apr 1;36(7):2284-5.
43. Ryckaert JP, Ciccotti G, Berendsen HJ. Numerical integration of the cartesian equations of motion of a system with constraints: molecular dynamics of n-alkanes. *Journal of computational physics*. 1977 Mar 1;23(3):327-41.
44. Saetang J, Chonpathompikunlert P, Sretrirutchai S, Roongsawang N, Kayasut K, Voravuthikunchai SP, Sukketsiri W, Tipmanee V, Sangkhathat S. Anti-cancer effect of engineered recombinant interleukin 18. *Advances in Clinical and Experimental Medicine: Official Organ Wroclaw Medical University*. 2020 Oct 8.
45. Saetang J, Puseenam A, Roongsawang N, Voravuthikunchai SP, Sangkhathat S, Tipmanee V. Immunologic function and molecular insight of recombinant interleukin-18. *PloS one*. 2016 Aug 2;11(8):e0160321.
46. Silva DA, Yu S, Ulge UY, Spangler JB, Jude KM, Labão-Almeida C, Ali LR, Quijano-Rubio A, Ruterbusch M, Leung I, Biary T. De novo design of potent and selective mimics of IL-2 and IL-15. *Nature*. 2019 Jan;565(7738):186-91.
47. Smyth MJ, Cretney E, Kershaw MH, Hayakawa Y. Cytokines in cancer immunity and immunotherapy. *Immunological reviews*. 2004 Dec;202(1):275-93.

48. Smyth MJ, Dunn GP, Schreiber RD. Cancer immunosurveillance and immunoediting: the roles of immunity in suppressing tumor development and shaping tumor immunogenicity. *Advances in immunology*. 2006 Jan 1;90:1-50.
49. Søndergaard CR, Olsson MH, Rostkowski M, Jensen JH. Improved treatment of ligands and coupling effects in empirical calculation and rationalization of pK<sub>a</sub> values. *Journal of chemical theory and computation*. 2011 Jul 12;7(7):2284-95.
50. Srivastava S, Pelloso D, Feng H, Voiles L, Lewis D, Haskova Z, Whitacre M, Trulli S, Chen YJ, Toso J, Jonak ZL, Chang HC, Robertson MJ. Effects of interleukin-18 on natural killer cells: costimulation of activation through Fc receptors for immunoglobulin. *Cancer Immunol Immunother*. 2013 Jun;62(6):1073-82.
51. Szilagyi A, Zhang Y. Template-based structure modeling of protein–protein interactions. *Current opinion in structural biology*. 2014 Feb 1;24:10-23.
52. Tarhini AA, Millward M, Mainwaring P, Kefford R, Logan T, Pavlick A, Kathman SJ, Laubscher KH, Dar MM, Kirkwood JM. A phase 2, randomized study of SB-485232, rhIL-18, in patients with previously untreated metastatic melanoma. *Cancer: Interdisciplinary International Journal of the American Cancer Society*. 2009 Feb 15;115(4):859-68.
53. Tse BW, Russell PJ, Lochner M, Förster I, Power CA. IL-18 inhibits growth of murine orthotopic prostate carcinomas via both adaptive and innate immune mechanisms. *PLoS One*. 2011 Sep 15;6(9):e24241.
54. Tsutsumi N, Kimura T, Arita K, Ariyoshi M, Ohnishi H, Yamamoto T, Zuo X, Maenaka K, Park EY, Kondo N, Shirakawa M. The structural basis for receptor recognition of human interleukin-18. *Nature communications*. 2014 Dec 15;5(1):1-3.
55. Swencki-Underwood B, Cunningham MR, Heavner GA, Blasie C, McCarthy SG, Dougherty T, Brigham-Burke M, Gunn GR, Goletz TJ, Snyder LA. Engineering human IL-18 with increased bioactivity and bioavailability. *Cytokine*. 2006 Apr 21;34(1-2):114-24.

56. Waldmann TA. Cytokines in cancer immunotherapy. *Cold Spring Harbor perspectives in biology*. 2018 Dec 1;10(12):a028472.
57. Wei H, Wang D, Qian Y, Liu X, Fan S, Yin HS, Wang X. Structural basis for the specific recognition of IL-18 by its alpha receptor. *FEBS letters*. 2014 Nov 3;588(21):3838-43.
58. Xue LC, Rodrigues JP, Kastritis PL, Bonvin AM, Vangone A. PRODIGY: a web server for predicting the binding affinity of protein–protein complexes. *Bioinformatics*. 2016 Dec 1;32(23):3676-8.
59. Yamamoto Y, Kato Z, Matsukuma E, Li A, Omoya K, Hashimoto K, Ohnishi H, Kondo N. Generation of highly stable IL-18 based on a ligand–receptor complex structure. *Biochemical and biophysical research communications*. 2004 Apr 23;317(1):181-6.
60. Yeung N, Lin YW, Gao YG, Zhao X, Russell BS, Lei L, Miner KD, Robinson H, Lu Y. Rational design of a structural and functional nitric oxide reductase. *Nature*. 2009 Dec;462(7276):1079-82.
61. Zhang H, Chen J. Current status and future directions of cancer immunotherapy. *Journal of Cancer*. 2018;9(10):1773.

## **APPENDICES**

## APPENDIX A

### AMBER INPUT FILES

#### 1. Topologies files preparation

##### 1.1 Topology files of IL-18 for MD simulation

```
>tleap
prot=loadpdb name.pdb
charge prot
solvatebox prot TIP3PBOX 14
addions prot Na+ 53
addions prot Cl- 53
setbox prot vdw
savepdb prot name-solv.pdb
charge prot
saveamberparm prot name-4-solv.prmtop name-start.rst7
```

#### 2. Input files for MD simulation of IL-18

##### 2.1 Energy minimization

```
- min-ntb1.in
minimize steepest descent 2000, conjugate gradient 1000
&cntrl
imin = 1,
maxcyc = 2000,
ncyc = 1000,
ntb = 1,
cut = 12,
ntxo = 1,
ioutfm = 1,
```

/

**2.2 Canonical (NVT) ensemble (force constants of 200 kcal · mol<sup>-1</sup>)**

- nvt200.in

Implicit solvent molecular dynamics

&amp;cntrl

imin=0, irest=0, ntx=1, ntr=1, ntxo=1,

ntpr=5000, ntwx=5000, nstlim=200000, ntwr=5000,

dt=0.001, ntt=3, tempi=10,

temp0=310, gamma\_ln=1.0, ig=-1,

ntp=0, ntc=2, ntf=2, cut=16,

ntb=1, ioutfm=0,

/

Hold the protein fixed

200.0

RES 1 156

END

END

**2.3 Canonical (NVT) ensemble (force constants of 100 kcal · mol<sup>-1</sup>)**

- nvt100.in

Implicit solvent molecular dynamics

&amp;cntrl

imin=0, irest=1, ntx=5, ntr=1, ntxo=1,

ntpr=5000, ntwx=5000, nstlim=200000, ntwr=5000,

dt=0.001, ntt=3, tempi=10,

temp0=310, gamma\_ln=1.0, ig=-1,

ntp=0, ntc=2, ntf=2, cut=16,

ntb=1, ioutfm=0,

/

Hold the protein fixed

100.0

RES 1 156

END

END

## 2.4 Canonical (NVT) ensemble (force constants of 50 kcal · mol<sup>-1</sup>)

- nvt50.in

Implicit solvent molecular dynamics

&cntrl

imin=0, irest=1, ntx=5, ntr=1, nt xo=1,

ntpr=5000, ntwx=5000, nstlim=200000, ntwr=5000,

dt=0.001, ntt=3, tempi=10,

temp0=310, gamma\_ln=1.0, ig=-1,

ntp=0, ntc=2, ntf=2, cut=16,

ntb=1, ioutfm=0,

/

Hold the protein fixed

50.0

RES 1 156

END

END

## 2.5 Canonical (NVT) ensemble (force constants of 25 kcal · mol<sup>-1</sup>)

- nvt20.in

Implicit solvent molecular dynamics

&cntrl

imin=0, irest=1, ntx=5, ntr=1, nt xo=1,

ntpr=5000, ntwx=5000, nstlim=200000, ntwr=5000,

dt=0.001, ntt=3, tempi=10,

temp0=310, gamma\_ln=1.0, ig=-1,

ntp=0, ntc=2, ntf=2, cut=16,

ntb=1, ioutfm=0,

/

Hold the protein fixed

25.0

RES 1 156

END

END

## 2.6 Canonical (NVT) ensemble (force constants of 10 kcal · mol<sup>-1</sup>)

- nvt10.in

Implicit solvent molecular dynamics

&cctrl

imin=0, irest=1, ntx=5, ntr=1, ntxo=1,

ntpr=5000, ntwx=5000, nstlim=200000, ntwr=5000,

dt=0.001, ntt=3, tempi=10,

temp0=310, gamma\_ln=1.0, ig=-1,

ntp=0, ntc=2, ntf=2, cut=16,

ntb=1, ioutfm=0,

/

Hold the protein fixed

10.0

RES 1 156

END

END

## 2.7 Isobaric-Isothermal (NPT) ensemble for 150 ns

### 2.7.1. md-npt-pre.in

NPT production 310K

&cctrl

imin=0,

ntx=5,

irest=1,

ntc=2,

ntf=2,

```
tol=0.0000001,  
nstlim=100000,  
ntt=1,  
temp0=310.0,  
ntpr=10000,  
ntwr=10000,  
ntwx=10000,  
dt=0.002,  
ig=-1,  
ntb=2,  
ntp=1,  
pres0=1.013,  
cut=16.0,  
ioutfm=0,  
ntxo=1,
```

```
/
```

### **2.7.2. md-npt.in**

NPT production 310K

&cntrl

```
imin=0,  
ntx=5,  
irest=1,  
ntc=2,  
ntf=2,  
tol=0.0000001,  
nstlim=75000000,  
ntpr=10000,  
ntwr=10000,  
ntwx=10000,  
dt=0.002,  
ig=-1,  
ntb=2,
```

```

ntp=1, ntt=1,
temp0=310.0, pres0=1.013,
cut=16.0,
ioutfm=0,
ntxo=1,
/

```

### 3. Script for MD simulation via AMBER 16

#### #### Minimize

```

pmemd.cuda -O -i min-ntbl.in -p name-solv.prmtop -c name-start.rst7
-r name-min.rst7 -o min-name.out

```

#### ##### NVT

```

pmemd.cuda -O -i nvt200.in -p name-solv.prmtop -c name-min.rst7 -r
name-res-200.rst7 -x name-res-200.nc -o name-res-200.out -ref name-
min.rst7

```

```

pmemd.cuda -O -i nvt100.in -p name-solv.prmtop -c name-res-200.rst7 -r
name-res-100.rst7 -x name-res-100.nc -o name-res-100.out -ref name-
min.rst7

```

```

pmemd.cuda -O -i nvt50.in -p name-solv.prmtop -c name-res-100.rst7 -r
name-res-50.rst7 -x name-res-50.nc -o name-res-50.out -ref name-min.rst7

```

```

pmemd.cuda -O -i nvt25.in -p name-solv.prmtop -c name-res-50.rst7 -r
name-res-25.rst7 -x name-res-25.nc -o name-res-25.out -ref name-min.rst7

```

```

pmemd.cuda -O -i nvt10.in -p name-solv.prmtop -c name-res-20.rst7 -r
name-res-10.rst7 -x name-res-10.nc -o name-res-10.out -ref name-min.rst7

```

**#### NPT**

```
pmemd.cuda -O -i md-npt-pre.in -p name-solv.prmtop -c name-res-10.rst7 -r  
npt-pre.rst7 -x solv-npt-pre.nc -o md-npt-pre.out
```

```
pmemd.cuda -O -i md-npt.in -p name-solv.prmtop -c npt-pre.rst7 -r npt-  
150ns.rst7 -x solv-npt-150ns.nc -o md-npt-150ns.out
```

## APPENDIX B

### FOLDX COMMAND LINES

#### 1. Structure preparation

##### 1.1 Energy minimization

<RepairPDB>

```
Foldx --command=RepairPDB --pdb=name.pdb --ionStrength=0.05 --pH=7 --  
water=CRYSTAL --vdwDesign=2 --pdbHydrogens=false --temperature=310
```

##### 2.2 Preparation of mutant models

<BuildModel>

```
Foldx --command=BuildModel --pdb=name.pdb --mutant-  
file=individual_list.txt --ionStrength=0.05 --pH=7 --water=CRYSTAL --  
vdwDesign=2 --pdbHydrogens=false --temperature=310 --numberOfRuns=5
```

#### 2. Binding free energy analysis

```
FoldX --command=AnalyseComplex --pdb=name.pdb --  
analyseComplexChains=A,B --temperature=310
```

## **APPENDIX C**

### **PROCEEDING**

**Prompat N**, Saetang J, Roongsawang N, Sangkhathat S, Tipmanee V. Structure-guided design of interleukin-18 as a potential cytokine-mediated immunotherapy. The 46th International Congress on Science, Technology and Technology-based Innovation (STT46), Ramkhamhaeng University, Bangkok, Thailand, 5-7 October 2020. (Oral presentation)



## E\_001\_OF

### E\_001\_OF: STRUCTURE-GUIDED DESIGN OF INTERLEUKIN-18 AS A POTENTIAL CYTOKINE-MEDIATED IMMUNOTHERAPY

Napat Prompat,<sup>1</sup> Jirakrit Saetang,<sup>1,2</sup> Niran Roongsawang,<sup>3</sup> Surasak Sangkhathat,<sup>2</sup> Varomyalin Tipmanee<sup>1,\*</sup>

<sup>1</sup> Department of Biomedical Sciences, Faculty of Medicine, Prince of Songkla University, Hat Yai, Songkhla 90110, Thailand

<sup>2</sup> Department of Surgery, Faculty of Medicine, Prince of Songkla University, Hat Yai, Songkhla 90110, Thailand

<sup>3</sup> Microbial Cell Factory Research Team, Biorefinery and Bioproduct Technology Research Group, National Center for Genetic Engineering and Biotechnology, National Science and Technology Development Agency, 113 Thailand Science Park, Phahonyothin Road, Khlong Nueng, Khlong Luang, Pathum Thani, 12120, Thailand

\*e-mail: tvaromya@medicine.psu.ac.th

#### Abstract:

In recent year, cytokine-mediated immunotherapy has rapidly emerged as an effective alternative approach for cancer treatment by modulating the host's anti-tumor response. Among the cytokine-based therapeutics, interleukin-18 (IL-18) has received considerable interest as a promising cancer therapeutic agent due to the ability of cytokine to inhibit cancer by enhancing natural killer cell (NK-cell) and cytotoxic T cell responses. Thus, there is considerable interest in developing IL-18 with advantageous properties. In this study, we used an integrated computational approach to design and predict the single point mutation of IL-18 binding residue for improving the biological activity. The potential amino acid substitution, N41D was chosen based on structural analysis of human IL-18 in complex with the receptors. The impacts of amino acid mutations on IL-18 structure and dynamic behavior were evaluated using atomistic molecular dynamics (MD) simulations via AMBER16 package. The results demonstrated that N41D mutation leads to an increase in flexibility while remaining the conformational stability, which was observed by the increase in the root mean square fluctuation of the residual level. Moreover, the N41D mutant showed predicted higher binding affinity than wild-type and E6K mutant (positive control) to the IL-18 receptors. Our present findings using *in silico* approaches suggest that the computationally designed IL-18 could be a promising candidate as a cytokine-based immunotherapeutic agent.

#### Introduction:

Cancer is a major cause of global death. In 2018, the World Health Organization (WHO) has reported an increase of 18.1 million cases and an estimated death rate of 9.6 million<sup>1</sup>. An increase of cancer patient has driven the development of new and more effective treatments. Immunotherapy, immune-based treatment that exploits patient's immune system to recognize and eliminate cancer, has emerged as a promising approach for cancer therapy and shown its great potential for treating human cancers due to selectivity and long-lasting effects<sup>2</sup>. The field of immunotherapy shows great progress toward a cancer treatment, such as immune checkpoint blockage agents, monoclonal antibodies, cancer vaccines, oncolytic viruses, adoptive cell therapy and especially, cytokine-mediated immunotherapy<sup>3</sup>.

The 46th International Congress on Science, Technology and Technology-based Innovation

601 | STT 46



Interleukin-18 (IL-18), an 18 kDa immunostimulatory cytokine primarily secreted by macrophages, is encoded by the *IL18* gene on chromosome 11q3.1<sup>4</sup>. This cytokine plays important roles in anti-tumor immune responses including the activation and proliferation of T cells, the induction of interferon- $\gamma$  (IFN- $\gamma$ ) production in natural killer cells (NK-cells), and the regulation of several cytokines in both innate and adaptive immunity against cancer cells, leading to the enhancement of patient's immune responses and tumor regression<sup>5</sup>. The binding modes of IL-18 and IL-18 receptors (IL-18R) play important roles to the biological function of the protein. The crystal structure of human IL-18 revealed that the binding sites are composed of two parts. The first part of binding site interact specifically with IL-18R $\alpha$  are site I and II, and site III is important for IL-18R $\beta$  receptor binding<sup>6</sup>.

The modification of amino acids on the binding sites of IL-18 through molecular cloning and mutagenesis techniques can enhance biological activity regarding the induction of IFN- $\gamma$  production in NK cells<sup>7</sup>. Targeting the binding sites and amino acid residues of IL-18 is an attractive strategy to improve the activity of this cytokine. However, *in vitro* study is enormously expensive, time-consuming and challenging to produce the recombinant engineered proteins effectively. Nowadays, computational-based protein design facilitates the discovery and development of novel protein with reduced cost-related and time-spent on the workbench. Therefore, we apply this computational technique to design and predict the biological activity enhancement of IL-18 so that the novel potential IL-18 will be obtained for immunotherapy alternative.

#### Methodology:

##### 1. *In silico* mutagenesis

Crystal structure of human IL-18 in complex with IL-18 receptor alpha, Protein Data Bank (PDB) code 3WO3, was chosen to use as the starting structure for amino acid modification in the protein sequence, as shown in Figure 1. To design the amino acid modification on the binding sites of IL-18, the surface amino acid residues within 6 angstroms to the receptor were selected based on the physicochemical properties including charge, size, and shape of residues.

The mutant model of the selected residue was mutated *in silico* using the PyMOL mutagenesis wizard<sup>8</sup>. IL-18 wild-type and two mutation models (E6K and M33Q) with experimental results from the previous study<sup>7</sup> were considered as a control group to validate the computational method. All protein structure visualization and rendering were performed using Visual Molecular Dynamics (VMD) version 1.9.3<sup>9</sup>.

##### 2. Molecular Dynamics (MD) simulations

After the generation of the model structures, MD simulations were performed using the AMBER 16 software package in order to mimic an *in vivo* condition and investigate the molecular dynamic behavior of the simulated structure. The model structures were subjected to energy minimization by LEaP module in AMBER 16 software package. PROPKA server was used to calculate the protonation state of protein at pH 7.4. Then, the protein solution system was neutralized by counter ions and solvated in TIP3P water molecules with 0.1M NaCl, then equilibrated at 310°K and pressure of 1 atm (1.013 bar). The system was simulated by 3ns NVT simulation with 1fs-time step and 100 ns. NPT simulation with 2fs-time step in AMBER16ieq force field using PMEMD in AMBER 16 software package<sup>10</sup>. Finally, Root-mean-square deviation (RMSD) and root-mean-square fluctuation (RMSF) of resulting structure were analyzed using cpptraj module in AMBER 16 software.

##### 3. Protein-protein docking and binding affinity assessment

After obtaining the minimized structures of each model, protein docking was performed using ClusPro 2.0 server<sup>11</sup> to generate the complex structures of the IL-18 mutant and IL-18 receptor based on rigid body docking, RMSD based clustering of the structures and refinement of selected structures. We selected the most optimal model and most likely native structures based on ClusPro 2.0 server scoring function. To assess the binding strength of these models, the complex structures were further submitted to PRODIGY webtools<sup>12</sup> to estimate the binding affinity of the complexes of IL-18/IL-18 receptor in term of binding free energy ( $\Delta G$ ) in kcal/mol and dissociation constant ( $K_d$ ) in molar units.

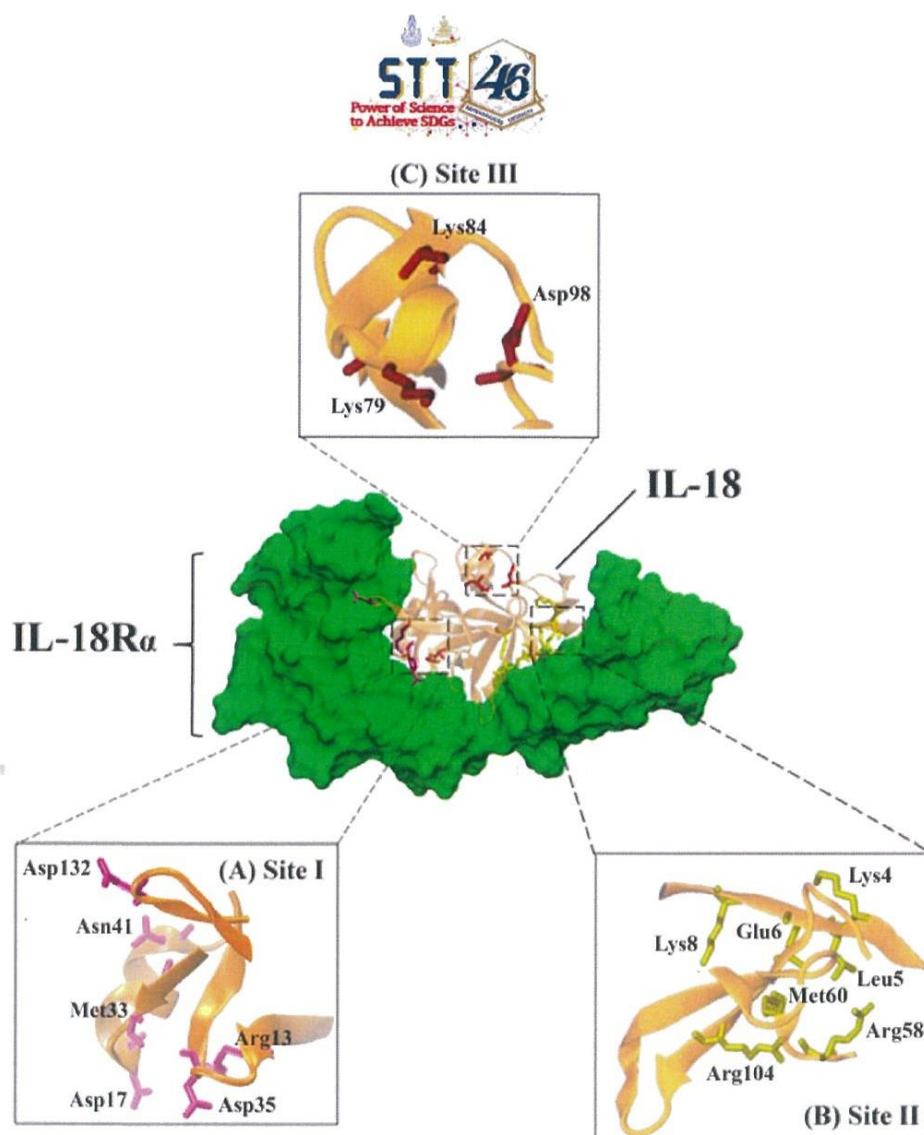


**Figure 1.** The structure of IL-18 (orange) and IL-18R $\alpha$  (green) binding complex (PDB ID: 3WO3). (A) Amino acids in the binding interface of IL-18 and IL-18R $\alpha$  as site I. (B) The binding residues in receptor binding site II. (C) The key residues in site III of IL-18 and its receptor, IL-18R $\beta$ .

#### Results and Discussion:

##### 1. *In silico* design of high affinity IL-18

Since the biological activity of IL-18 regarding the induction of IFN- $\gamma$  production in the immune cells, especially NK-cells<sup>5</sup> required the specific binding to its receptors through the residues that dominated at site I (Asp17, Met33, Asp35, Asn41) and II (Glu6, Lys53, Met60), the alteration of these contact residues may affect the biological function of IL-18. Through analyzing the interaction between IL-18 and its receptors, we initially found that Asn41 in site I is surrounded by positively charged amino acid (Arg25 and His27) on the surface of IL-18R $\alpha$ , as shown in Figure 2A. With the aim of improving the binding interaction of IL-18, Asn41 was substituted by Asp to facilitate the binding affinity by using electrostatic forces and surface charge complementarity, as shown in Figure 2B.

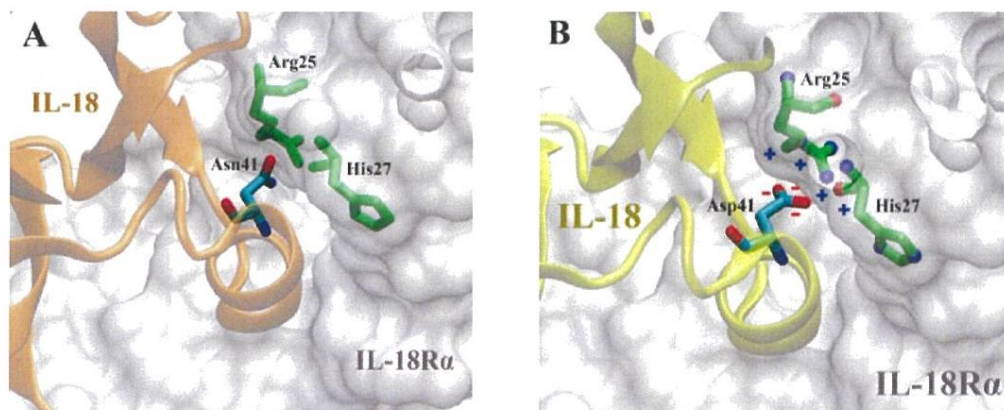


**Figure 2.** Structural comparison between wild-type (orange) and N41D mutant (yellow). Figure 2(A) shows the Asn41<sup>IL-18</sup> directly interacts with positively charged amino acid side chains of IL-18R $\alpha$  though electrostatic interactions. Figure 2(B) shows the molecular interaction between the mutated structure, N41D and IL-18R $\alpha$  at site I (white).

## 2. Conformational stability analysis

To investigate the mutational effect on the conformational stability of the wild-type and mutant structures, RMSD values were calculated using the final 100 ns trajectories of equilibration MD simulations. As shown in Figure 3, the wild-type and mutant structures (E6K, M33Q and N41D) showed almost a similar pattern in terms of the RMSD values during a simulation time of 100 ns. The RMSD value below 3 Å is acceptable. In addition, the averaged RMSD values of the wild-type, E6K, M33Q and N41D mutant were 1.63, 1.49, 1.82 and 1.45 Å, respectively. A small variation in the average RMSD values of wild-type and N41D mutant after MD simulations lead to the conclusion that the mutation of Asn-41 to aspartic acid had no effect on the overall conformation and folding of protein.

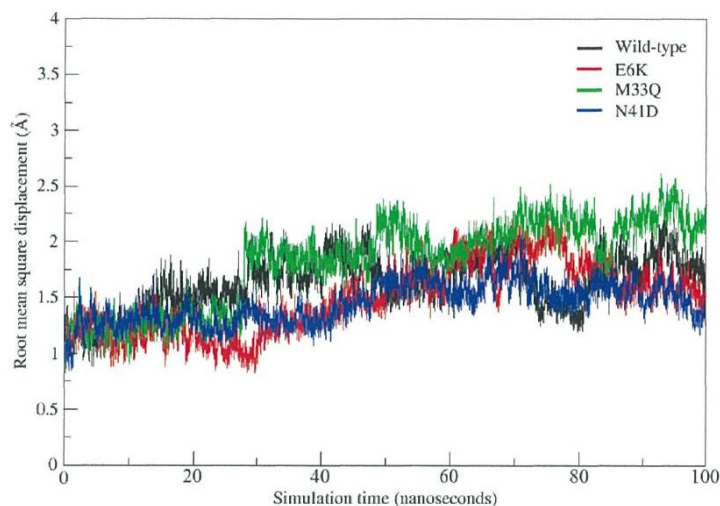


**Figure 3.** Root-mean-square deviation (RMSD) from MD simulation of all IL-18 structures in Angstrom units. Wild-type (black), E6K (red), M33Q (green), and N41D (blue).

### 3. Structural flexibility analysis

To determine the effect of the substituted amino acid on the dynamic behavior of the IL-18 residues, the structural flexibility of protein was reported as the RMSF plot in Figure 4. Analysis of fluctuation based on the RMSF values revealed that the flexibility of amino acid residues of the mutants E6K and M33Q have been altered when compared to wild-type, which was in agreement with the activity changes of E6K and M33Q mutant described in the previous experimental study<sup>7</sup>. Surprisingly, the activity of E6K was increased whereas decreasing in the mutant M33Q. This implies that a higher fluctuation in residues of M33Q mutant may disrupt the binding interaction of IL-18 and its receptors resulting in the activity loss of M33Q, which we discuss in detail in a subsequent section. In this study, the presence of higher RMSF value in the mutant N41D protein was observed when compared to wild-type at residue 90<sup>th</sup>-95<sup>th</sup> in the loop region connecting  $\beta$ 7 sheet, which plays an important role in the binding interaction of IL-18 and IL-18R $\alpha$  site I. This result suggests that N41D mutation may affect the biological activity of IL-18.

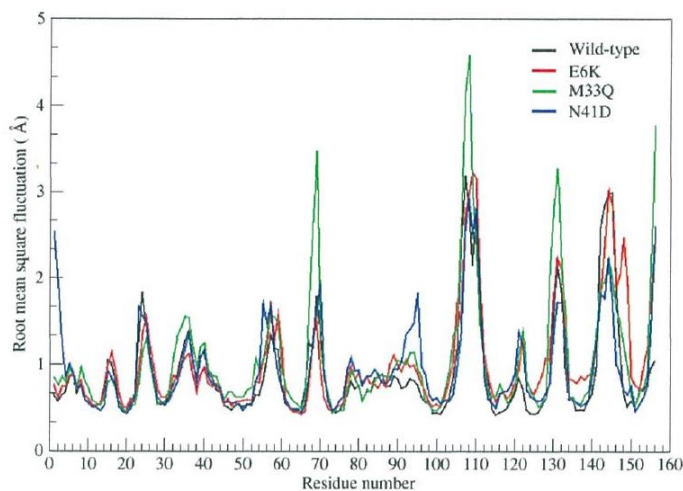


**Figure 4.** Root-mean-square fluctuation (RMSF) from MD simulation of all IL-18 structures in Angstrom units. Wild-type (black), E6K (red), M33Q (green), and N41D (blue).

#### 4. Molecular docking study and binding affinity evaluation

To evaluate the binding affinity of IL-18 mutant N41D against wild-type and other two control mutants E6K and M33Q. The docking process was conducted by using ClusPro 2.0 server. The binding affinity of protein-protein complexes was determined using PRODIGY server. The predicted value of binding free energy ( $\Delta G$ ) and dissociation constant ( $K_d$ ) of docking results are shown in Table 1. Our computational study demonstrated that the binding affinity of IL-18 wild-type, E6K, and M33Q mutants in the control group was consistent with their biological activities in the previous experimental study<sup>7</sup>. In this work, the computationally designed IL-18 with N41D mutation showed the strongest binding affinity with  $\Delta G = -15.6$  kcal/mol and better dissociation constant ( $K_d$ ) of  $9.40 \times 10^{-12}$  molar compared to wild-type and E6K mutant (positive control) with lesser affinity  $-14.1$  kcal/mol and  $-15.4$  kcal/mol respectively. These results suggested that the substitution of Asn41 to aspartic acid may improve IL-18 activity by increasing anionicity in N41D. In contrast, the increasing flexibility at the residual level of M33Q mutant (negative control), as mentioned earlier, may result in the loss of the binding interaction between IL-18 and its receptor since the decrease in binding affinity was observed in the M33Q mutant when compared to wild-type. These findings implied that conformational flexibility and binding affinity are responsible for the biological activity of IL-18. Further studies are required to produce the computationally designed IL-18 through protein expression system and examine its ability to enhance the IFN- $\gamma$  production in NK-92MI cells via cell culture and immunologic measurement. Therefore, if the designed IL-18 exhibits potent activity with increased IFN- $\gamma$  production compared to wild-type, it would be a promising candidate as a cytokine-based immunotherapy.



**Table 1.** Binding affinities and biological activities of wild-type and mutant IL-18 structures.

Mutation	Predicted $\Delta G$ (kcal/mol)	Predicted $K_d$ (M)	Binding affinity	Biological activity <sup>a</sup>
<i>Control group</i>				
Wild-type	-14.1	$1.10 \times 10^{-10}$	Standard	Standard
E6K	-15.4	$1.50 \times 10^{-11}$	Increase	Increased activity
M33Q	-13.4	$3.90 \times 10^{-10}$	Decrease	Decreased activity
N41D	-15.6	$9.40 \times 10^{-12}$	Increase	Predicted increase

<sup>a</sup>The biological activity of E6K and M33Q mutants were evaluated experimentally by the measurement of IFN- $\gamma$  production in NK-92MI cells when compared to IL-18 wild-type<sup>7</sup>.

#### Conclusion:

In summary, we have proposed a therapeutic protein design strategy to improve the biological activity of IL-18 which was based on structural, dynamic and energetic analyses of the interaction between IL-18 and IL-18 receptor. Preliminary, the mutation at the binding residue asparagine 41 (N41D) majorly affected the flexibility and binding affinity of IL-18. Our present findings using *in silico* study demonstrate that the computationally designed IL-18 could be considered as a potential therapeutic candidate for cancer treatment. However, the impacts of the designed protein on IL-18 activity need to be validated experimentally.

#### Acknowledgements:

This work was supported by the government budget of Prince of Songkla University (Grant No. SCI6101034M). In addition, we would like to acknowledge the Central Research Laboratory, Faculty of Medicine, Prince of Songkla University for providing necessary laboratory facilities.

#### References:

1. Bray F, Ferlay J, Soerjomataram I, Siegel RL, Torre LA, Jemal A. CA. 2018;394-424.
2. Zhang H, Chen J. J Cancer. 2018;9:1773-1781.
3. Berraondo P, Sanmamed MF, Ochoa MC, Iñaki E, Maria AA, José LP, et al. Br J Cancer. 2019;120:6-15.
4. Yasuda K, Nakanishi K, Tsutsui H. Int J Mol Sci. 2019;20:649.
5. Tsutsui H, Nakanishi K. Immunotherapy. 2012;4:1883-1894.
6. Tsutsumi N, Kimura T, Arita K, Ariyoshi M, Ohnishi H, Yamamoto T, et al. Nat Commun. 2014;5:5340.
7. Saetang J, Puseenam A, Roongsawang N, Voravuthikunchai S, Sangkhathat S, Tipmanee V. PLoS One. 2016;11:e0160321.
8. Rigsby RE, Parker AB. Biochem Mol Biol Educ. 2016;4:433-437.
9. Humphrey W, Dalke A, Schulten K. J. Mol. Graph. 1996;14:33-38, 27-28.
10. Case A, Cheatham E, Darden T, Gohlke H, Luo RJ. Comput. Chem. 2005;26:1668-1688.
11. Kozakov D, Hall DR, Xia B, Porter KA, Padhorna D, Yueh C, et al. Nat Protoc. 2017;12:255-278.
12. Xue L, Rodrigues J, Kastritis P, Bonvin A, Vangone A. Bioinformatics, 2016;32:3676-3678.

## VITAE

**Name** Mr. Napat Prompat

**Student ID** 6110320017

### **Educational Attainment**

<b>Degree</b>	<b>Name of institution</b>	<b>Year of Graduation</b>
Bachelor of Science (Medical Technology)	Prince of Songkla University	2018

### **Scholarship Award during Enrolment**

Research Grant, Faculty of Medicine, Prince of Songkla University

### **List of Publication and Proceeding**

1. **Prompat N**, Saetang J, Roongsawang N, Sangkhathat S, Tipmanee V. Structure-guided design of interleukin-18 as a potential cytokine-mediated immunotherapy. The 46th International Congress on Science, Technology and Technology-based Innovation (STT46), Ramkhamhaeng University, Bangkok, Thailand, 5-7 October 2020. (Oral presentation)
2. **Prompat N**, Saetang J, Roongsawang N, Sangkhathat S, Tipmanee V. Structure-guided design of interleukin-18 as a potential cytokine-mediated immunotherapy. The 7th Joint symposium BME-BMS-EU-HS (JSPG 2020) Post-graduate Health Science and Technology Conference, 3-4 September 2020. (Oral presentation)